

10. SITE 665¹

Shipboard Scientific Party²

HOLE 665A

Date occupied: 3 April 1986, 2100 UTC
Date departed: 4 April 1986, 1807 UTC
Time on hole: 20.9 hr
Position: 2°57.07'N, 19°40.07'W
Water depth (sea level; corrected m, echo-sounding): 4746
Water depth (rig floor; corrected m, echo-sounding): 4756.5
Bottom felt (rig floor; m, drill pipe measurement): 4750.9
Distance between rig floor and sea level (m): 10.5
Total depth (rig floor, m): 4848.8
Penetration (m): 97.9
Number of cores (including cores with no recovery): 11
Total length of cored section (m): 97.9
Total core recovered (m): 99.9
Core recovery (%): 102.1
Oldest sediment cored:
Depth (mbsf): 97.9
Nature: red clay
Age: early Pliocene (>4.6 Ma)

HOLE 665B

Date occupied: 4 April 1986, 1955 UTC
Date departed: 5 April 1986, 0815 UTC

Time on hole: 12.3 hr
Position: 2°57.07'N, 19°40.07'W
Water depth (sea level; corrected m, echo-sounding): 4746
Water depth (rig floor; corrected m, echo-sounding): 4756.5
Bottom felt (rig floor; m, drill pipe measurement): 4752.3
Distance between rig floor and sea level (m): 10.5
Total depth (rig floor, m): 4834.3
Penetration (m): 82.0
Number of cores (including cores with no recovery): 9
Total length of cored section (m): 82
Total core recovered (m): 72.4
Core recovery (%): 88.3
Oldest sediment cored:
Depth (mbsf): 82.0
Nature: red clay
Age: early Pliocene (>4.6 Ma)

Principal results: Site 665 is located in the eastern equatorial Atlantic at 2°57.07'N, 19°40.07'W, in a water depth of 4740.4 m in relatively flat terrain along the base of the southeastern margin of the Sierra Leone Rise (see "Background and Scientific Objectives" section, this chapter). The site is situated in a region of well-stratified, flat-lying, moderately reflective layers that are draped partly over acoustic basement, but also tend to have filled in the deeper basement lows (see "Background and Scientific Objectives" section, this chapter). Our primary objective was to obtain a Pliocene-Pleistocene sequence for use as part of a depth transect to study deep-water isolation in the eastern equatorial Atlantic. Our secondary objective was to monitor long-term fluxes in CaCO₃ from surface waters, along with CaCO₃ dissolution and downslope redistribution.

From Holes 665A and 665B, we recovered a total of 20 advanced piston corer (APC) cores to depths of 97.9 and 82.0 meters below seafloor (mbsf), respectively (Table 1). Both holes were cored continuously. Recovery averaged 102.1% for Hole 665A and 88.3% for Hole 665B.

The sedimentary sequence at Site 665 is divided into two lithologic units (Fig. 1). From 0 to 72.5 mbsf, the lithology of Unit I is cyclical nannofossil and clay-bearing nannofossil oozes of late Pliocene through Holocene age (4.1 to 0.0 Ma). Carbonate content varies from 0% to 80%, and a trend toward deeper CaCO₃ minima exists near the top of the unit (see "Organic Geochemistry" section, this chapter). From 72.5 to 97.9 mbsf, lithologic Unit II is red clay of lower Pliocene (5.0 to 4.1 Ma) age and may be older in the nonfossiliferous lower section. No CaCO₃ is found in this layer, except in a few turbidite beds brought in from shallower depths.

Opaline silica is a secondary component of both units, except for some 10-cm-thick diatom ooze layers in the uppermost 20 m of Unit I (1 to 0 Ma). Organic carbon is less than 1% of the sediment but is consistently more abundant in the upper 50 m of the upper lithologic unit. Several sharp unburrowed contacts were observed in each unit; these probably indicate erosion by bottom currents. Several such units toward the bottom of lithologic Unit I (~60–70 mbsf) had increased manganese contents, suggesting significant periods of non-deposition or slow deposition.

The paleomagnetic stratigraphy at Sites 665 was excellent, with clear definition of all chrons and subchrons down to the Gauss (see "Paleomagnetism" section, this chapter). Nannofossil and planktonic-foraminifer stratigraphy also was good through the late Pliocene and Pleistocene, despite moderately severe dissolution. Dia-

¹ Ruddiman, W., Sarnthein, M., Baldauf, J., et al., 1988. *Proc., Init. Repts. (Pt. A), ODP*, 108.

² William Ruddiman (Co-Chief Scientist), Lamont-Doherty Geological Observatory, Palisades, NY 10964; Michael Sarnthein (Co-Chief Scientist), Geologisch-Paläontologisches Institut, Universität Kiel, Olshausenstrasse 40, D-2300 Kiel, Federal Republic of Germany; Jack Baldauf, ODP Staff Scientist, Ocean Drilling Program, Texas A&M University, College Station, TX 77843; Jan Backman, Department of Geology, University of Stockholm, S-106 91 Stockholm, Sweden; Jan Bloemendal, Graduate School of Oceanography, University of Rhode Island, Narragansett, RI 02882-1197; William Curry, Woods Hole Oceanographic Institution, Woods Hole, MA 02543; Paul Farrimond, School of Chemistry, University of Bristol, Cantocks Close, Bristol BS8 1TS, United Kingdom; Jean Claude Faugeres, Laboratoire de Géologie-Océanographie, Université de Bordeaux I, Avenue des Facultés, Talence 33405, France; Thomas Janacek, Lamont-Doherty Geological Observatory, Palisades, NY 10964; Yuzo Katsura, Institute of Geosciences, University of Tsukuba, Ibaraki 305, Japan; Hélène Manivit, Laboratoire de Stratigraphie des Continents et Océans, (UA 319) Université Paris VI, 4 Place Jussieu, 75230 Paris Cedex, France; James Mazzullo, Department of Geology, Texas A&M University, College Station, TX 77843; Jürgen Miener, Geologisch-Paläontologisches Institut, Universität Kiel, Olshausenstrasse 40, D-2300 Kiel, Federal Republic of Germany, and Woods Hole Oceanographic Institution, Woods Hole, MA 02543; Edward Pokras, Lamont-Doherty Geological Observatory, Palisades, NY 10964; Maureen Raymo, Lamont-Doherty Geological Observatory, Palisades, NY 10964; Peter Schultheiss, Institute of Oceanographic Sciences, Brook Road, Wormley, Godalming, Surrey GU8 5UG, United Kingdom; Rüdiger Stein, Geologisch-Paläontologisches Institut, Universität Giessen, Senckenbergstrasse 3, 6300 Giessen, Federal Republic of Germany; Lisa Tauxe, Scripps Institution of Oceanography, La Jolla, CA 92093; Jean-Pierre Valet, Centre de Faibles Radioactivités, CNRS, Avenue de la Terrasse, 91190 Gif-sur-Yvette, France; Philip Weaver, Institute of Oceanographic Sciences, Brook Road, Wormley, Godalming, Surrey GU8 5UG, United Kingdom; Hisato Yasuda, Department of Geology, Kochi University, Kochi 780, Japan.

toms were generally not stratigraphically useful because of poor preservation, except for the thin layers in the upper unit.

Depositional rates average 15 to 24 m/m.y. from 3.0 to 0.0 Ma in the upper Pliocene and Pleistocene nannofossil-ooze cycles of the upper lithologic unit but only 4 m/m.y. in the red clay. Between-hole correlations, based on paleomagnetic susceptibility data, verify the continuity of the composite section to a depth of 68 mbsf (about 3.5 Ma).

The increasing amplitude of the Pliocene-Pleistocene CaCO₃ cycles at Site 665 (Fig. 1), accompanied by increasing organic carbon and opaline silica, is similar to trends observed at other sites during Leg 108. The Sierra Leone Rise is located in an area marked today by relatively low productivity, with higher productivity toward both the north (the northwest African coastal upwelling regime) and the south (the equatorial divergence region). Nevertheless, the climatic indicators available for shipboard analysis at Site 665 suggest the same basic trend toward some combination of higher silica productivity, higher terrigenous dilution, lower carbonate productivity, or stronger carbonate dissolution through the late Pliocene and Pleistocene.

At Site 665, the early Pliocene shift in the carbonate compensation depth (CCD), marked by the onset of CaCO₃ sedimentation,

Table 1. Site 665 coring summary (drilling depths).

Core no./type	Date (April 1986)	Time (UTC)	Depths (mbsf)	Length cored (m)	Length recovered (m)	Recovery (%)
108-665A-1H	4	0720	0-2.9	2.9	2.9	100.0
108-665A-2H	4	0820	2.9-12.4	9.5	9.6	101.0
108-665A-3H	4	0930	12.4-21.9	9.5	9.8	103.0
108-665A-4H	4	1035	21.9-31.4	9.5	9.9	104.0
108-665A-5H	4	1145	31.4-40.9	9.5	9.7	102.0
108-665A-6H	4	1300	40.9-50.4	9.5	9.9	103.0
108-665A-7H	4	1357	50.4-59.9	9.5	9.6	100.0
108-665A-8H	4	1459	59.9-69.4	9.5	9.4	98.6
108-665A-9H	4	1600	69.4-78.9	9.5	9.6	101.0
108-665A-10H	4	1703	78.9-88.4	9.5	9.9	104.0
108-665A-11H	4	1807	88.4-97.9	9.5	9.8	103.0
108-665B-1H	4	2040	0-6.0	6.0	6.0	100.0
108-665B-2H	4	2128	6.0-15.5	9.5	9.8	103.0
108-665B-3H	4	2239	15.5-25.0	9.5	9.4	98.5
108-665B-4H	4	2353	25.0-34.5	9.5	9.7	102.0
108-665B-5H	5	0110	34.5-44.0	9.5	9.7	102.0
108-665B-6H	5	0230	44.0-53.5	9.5	9.7	102.0
108-665B-7H	5	0330	53.5-63.0	9.5	7.9	82.7
108-665B-8H	5	0445	63.0-72.5	9.5	0	0
108-665B-9H	5	0815	72.5-82.0	9.5	10.3	108.2

H = hydraulic piston. UTC = Universal Time Coordinated.

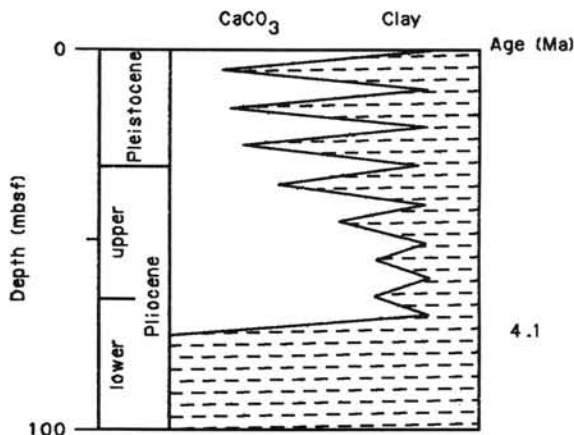


Figure 1. Biostratigraphic and lithostratigraphic summary of Site 665. Dashed pattern indicates clay with secondary silica and minor organic-carbon contents. Schematic CaCO₃ cycles indicate decreasing CaCO₃ and increasing clay (and opaline silica) contents from the late Pliocene to the late Pleistocene.

occurs between 4.6 and 3.8 Ma (see "Organic Geochemistry" section, this chapter). This age compares with that of a similar shift observed at other Leg 108 sites.

BACKGROUND AND SCIENTIFIC OBJECTIVES

Site 665 (target site Eq-6) is one of four sites in a transect taken at different water depths down the southern margin of the Sierra Leone Rise (Fig. 2). We planned two major kinds of objectives at Site 665.

The first group of objectives centered on the use of this site as the deep end member of a late Neogene bathymetric transect on the southern Sierra Leone Rise. Studies of late Pleistocene sediments in conventional piston cores by Curry and Lohmann (1983) have shown that water below about a 3800-m depth in the eastern Atlantic was more isolated from water at the same depths in the western Atlantic than is the case today. This isolation is suggested by a 0.7‰ depletion of δ¹³C values in benthic foraminifers in the eastern basin and by a higher organic-carbon content in the deeper cores.

Thus, our primary objective in the Sierra Leone Rise transect was to retrieve a suite of cores located close together in space but that spanned a greater depth range to trace these intervals of increased isolation back into the Neogene. For this purpose, Site 665 was critical because it lies well below the 3800-m water depth at which relative isolation of the eastern Atlantic deep circulation becomes evident.

A secondary depth-related objective was to use this closely spaced group of cores to monitor long-term fluxes of CaCO₃ (both bulk calcareous nannofossils and planktonic foraminifers, as well as individual species of planktonic foraminifers), the dissolution of CaCO₃, and the downslope movement of carbonate and noncarbonate fractions. This followed a strategy applied to gravity cores spanning the last 160,000 yr by Curry and Lohmann (1984).

A third objective at Site 665 was to measure late Neogene fluxes of eolian dust and freshwater diatoms as indicators of continental source-area aridity and of wind strength.

Geologic and Topographic Setting

Site 665 is located in the eastern equatorial Atlantic in relatively level terrain along the base of the southeastern margin of the Sierra Leone Rise (Figs. 2 and 3). Jacobi and Hayes (1982) described the Sierra Leone Rise as an aseismic system of plateaus probably formed at the mid-Atlantic Ridge crest during a phase of excess basalt generation.

Air-gun records from this region show at least 0.8 s of sediment above acoustic basement (Figs. 4 and 5), although this basement is obscured in the immediate vicinity of Site 665 because of the thick sedimentary cover. Acoustic reflectors are well stratified and moderately reflective. The sediment appears to be draped fairly conformably over the acoustic basement, indicating mainly pelagic deposition. Sediment thickness varies with basement relief, suggesting some net infilling of the low relief by relatively gentle redepositional processes. Echograms from Site 665 show relatively flat, reflective layering but also suggest the possible presence of small-scale vertical faulting in certain places along the track line.

The basement age at Site 665 is Cretaceous (about 80 Ma), based on the regional magnetic lineations and on previous drilling results. The sediment section in the upper 80 m is lower Pliocene to Holocene nannofossil oozes and clays, with clay below.

OPERATIONS

From Site 664, we steamed at 13 kt along a course of 069° toward Site 665. At 1700 UTC on 3 April 1986, we reached a way point at 2°47'N, 19°30'W (see Fig. 2; "Background and Scientific Objectives" section, this chapter). (All times are Universal Time Coordinated, formerly expressed as GMT,

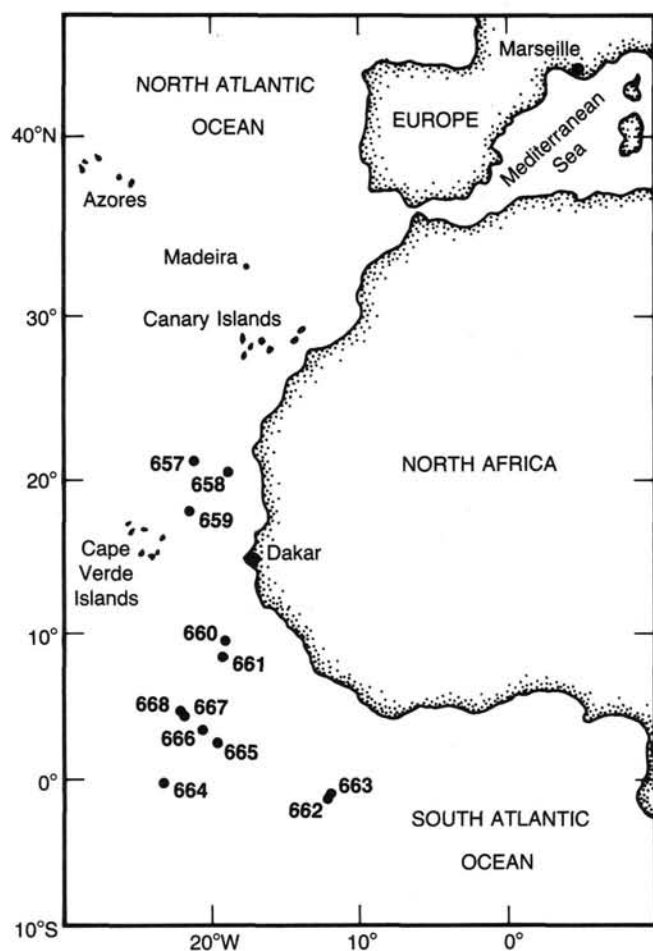


Figure 2. Locations of Leg 108 sites.

Greenwich Mean Time.) We turned to a course of 312° , slowed to 5 kt, and streamed out our 80-in.³ water gun and a magnetometer. After initial trouble receiving the water-gun signal, all systems were working by 1730. We continued along the same course until 2005, when we reached $2^\circ 58.3' N$, $19^\circ 42.58' W$. We then turned to a course of 144° and followed it to the eventual location of Site 665 at $2^\circ 57.07' N$, $19^\circ 40.07' W$. We dropped a beacon at 2050, brought in the geophysical gear, returned over the beacon by 2100 on 3 April, and began running drill pipe into Hole 665A.

The first advanced piston corer (APC) cores came on deck at 0720 on 4 April, and we cored continuously with the APC. The last APC core (108-665A-11H), which reached a penetration depth of 97.9 mbsf, came on deck at 1807. Recovery for Hole 665A averaged 102.1%. We then pulled out of Hole 665A and offset the drill string at Hole 665B.

We spudded in Hole 665B at 1955 on 4 April, and the first APC core came on deck at 2040. We cored continuously with the APC, reaching a penetration depth of 82.0 mbsf with the final APC core (108-665B-9H), which came on deck at 0815 on 5 April. Recovery at Hole 665B averaged 88.3%, with the lower value mainly caused by the total loss of Core 108-665B-8H. All cores in Hole 665B were oriented, and heat flow was measured for Cores 108-665B-4H, -665B-6H, and -665B-9H.

We began pulling out of Hole 665B at 0900. The drill string was on deck by 1700, and we were under way to Site 666 at 1718 on 5 April.

The weather was initially good at Site 665, but a squall blew up with winds of up to 50 kt and sustained winds of 30–40 kt

during coring of Hole 665B from about 2100 on 4 April until 0300 on 5 April. The sea state was only slightly turbulent with minor rolling of the ship and no perceptible pitching.

LITHOSTRATIGRAPHY AND SEDIMENTOLOGY

Introduction

Two major stratigraphic units were recognized at Site 665 (Fig. 6). Unit I is composed of nannofossil ooze and foraminifer-nannofossil oozes of early Pliocene and Pleistocene age (4.1–0 Ma). Unit II is composed of red clay of early Pliocene age (5.0–4.1 Ma) and possibly older. Each sedimentary unit is described in detail next.

Unit I

Cores 108-665A-1H to -665A-8H, CC; depth, 0–69.4 mbsf; age, early Pliocene to Holocene.

Cores 108-665B-1H to -665B-8H, CC; depth, 0–72.5 mbsf; age, early Pliocene to Holocene.

Unit I is composed primarily of interbedded nannofossil and foraminifer-nannofossil oozes. Muddy nannofossil, siliceous nannofossil, and diatom oozes are scattered in the upper section of this unit. These oozes are white, light gray, gray, yellowish brown, and brown. The diatom ooze is dark olive gray to very dark gray. Bioturbation is moderate to extensive throughout the unit. Purple, black, and grayish green microlaminations are scattered. A few thin turbidites interrupt the pelagic deposits.

The carbonate content of the unit generally varies from 30% to 80%, with a few intervals in the upper 30 m having no detectable carbonate (Fig. 6). These noncarbonate intervals are diatom oozes approximately 10 cm thick. Diatoms, radiolarians, and sponge spicules are the primary biogenic siliceous components in the nannofossil and foraminifer-nannofossil oozes. The combined concentration of the siliceous components in these calcareous oozes decreases from about 35% in the upper few meters to trace amounts at 30 mbsf. The terrigenous component is composed primarily of clay (5%–30%) and quartz (5%–25%) but does not appear to exhibit the same overall decrease in concentration with depth as does the siliceous component.

Unit II

Cores 108-665A-9H to -665A-11H, CC; depth, 69.4–97.9 mbsf; age, early Pliocene.

Cores 108-665B-9H to -665B-9H, CC; depth, 72.5–82.0 mbsf; age, early Pliocene.

Unit II is composed of silt-bearing clay generally barren of microfossils. This clay ranges in color from light yellowish brown to dark yellowish brown. The sediment is extensively bioturbated and exhibits abundant manganese staining. Clay (85%–90%) and quartz (5%–10%) are the primary components of this unit, with accessory minerals (feldspars, zeolites, and micas) present in trace amounts (0%–5%).

Depositional History

The stratigraphic sequence at Site 665 records large changes in the carbonate compensation depth (CCD) and changes in the productivity of equatorial surface waters. Before 4.1 Ma, this site was below the CCD and was characterized by slow deposition of pelagic clays. Carbonate deposition in the interval occurred only by the rapid deposition of two thin, carbonate-rich turbidites. At approximately 4.1 Ma, the rapid lowering of the CCD resulted in the deposition of a sequence of nannofossil and foraminifer-nannofossil oozes. The deposition of these oozes continues to this day (12 April 1986). Little or no siliceous material and organic carbon were deposited from 4.1 to 2.5 Ma. Organic-carbon preservation increased at about 2.5 Ma (50 mbsf, Fig. 6), whereas biogenic opal preservation increased at about

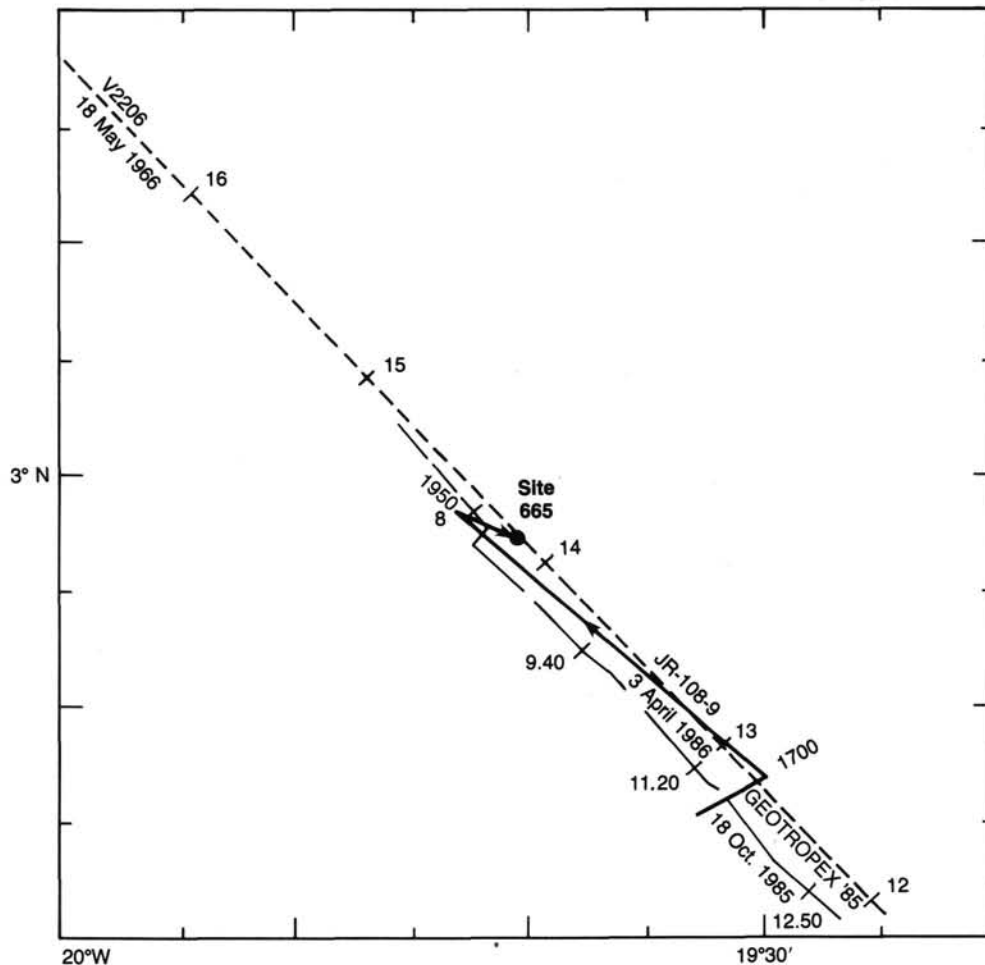


Figure 3. Seismic track lines near Site 665.

1.5 Ma (30 mbsf, Fig. 6). The increase in organic-carbon preservation was the result of increased productivity in the surface waters or increased preservation because of reduced oxygen conditions in the deep water. The increase in biogenic opal preservation indicates an increase in surface-water productivity that resulted in generally increased deposition rates for the interval 1.5 Ma through the present.

BIOSTRATIGRAPHY

Two holes were drilled at Site 665, in a water depth of 4740.4 m: Hole 665A to 97.9 mbsf and Hole 665B to 82.0 mbsf. Both holes contained a continuous biostratigraphic record of the lower Pliocene through Holocene, and little evidence exists of the slumps and turbidites that characterized the previous few holes (Site 662, 663, and 664) (Figs. 7 and 8). The only reworked specimens identified were found in nannofossil assemblages in the red-clay facies at the bottom of the holes.

Generally, the calcareous assemblages of this site exhibit moderate-to-poor preservation. Calcareous nannofossils are abundant, and the assemblages are characterized by tropical species with abundant discoasters. Planktonic foraminifers range from common to few and show moderate-to-poor preservation. Assemblages are tropical in composition, with few of the temperate species that characterized Site 662 and 663. The lower Pliocene red clays (below 70 mbsf) are barren of planktonic foraminifers. Benthic foraminifers are few to rare, with moderate-to-poor preservation in the Pleistocene, and common in the upper Pliocene,

with good preservation. Variations in the upper Pliocene assemblages seem to indicate that changes in composition of bottom-water masses were occurring at that time. As with the other calcareous microfossils, benthic foraminifers are absent below Core 108-665A-9H.

Diatoms were rare at this site and invariably with poor preservation. Below Cores 108-665A-5H and -665B-6H, the sediment was barren of diatoms, except in Section 108-665A-11H, CC. Above this level, few age-diagnostic species were observed. Rare, freshwater diatoms occurred in some core-catcher samples.

Calcareous Nannofossils

Both holes drilled at Site 665 exhibit a continuous, normal biostratigraphic sequence from the lower Pliocene through Holocene. Below Sample 108-665-9H-5, 135 cm, the sediments are barren of nannofossils. However, Sections 108-665A-9H-4 and -665A-9H-5 contain mixed assemblages, except Sample 108-665A-9H-4, 135 cm, which is barren, and Sample 108-665A-9H-5, 32 cm, which shows an extensively dissolved basal Pliocene assemblage without older contaminants. Eocene and Miocene forms are mixed in Sample 108-665A-9H-5, 25 cm (e.g., co-occurrence of *Coccolithus formosus*, *Discoaster barbadiensis*, *Discoaster quinqueramus*, and *Reticulofenestra umbilicus*), whereas Paleocene, middle and late Miocene, and Pliocene forms are mixed in Sample 108-665A-9H-5, 135 cm (*Discoaster multiradiatus*, *Discoaster kuqleri*, *Discoaster neohamatus*, *D. quinquera-*

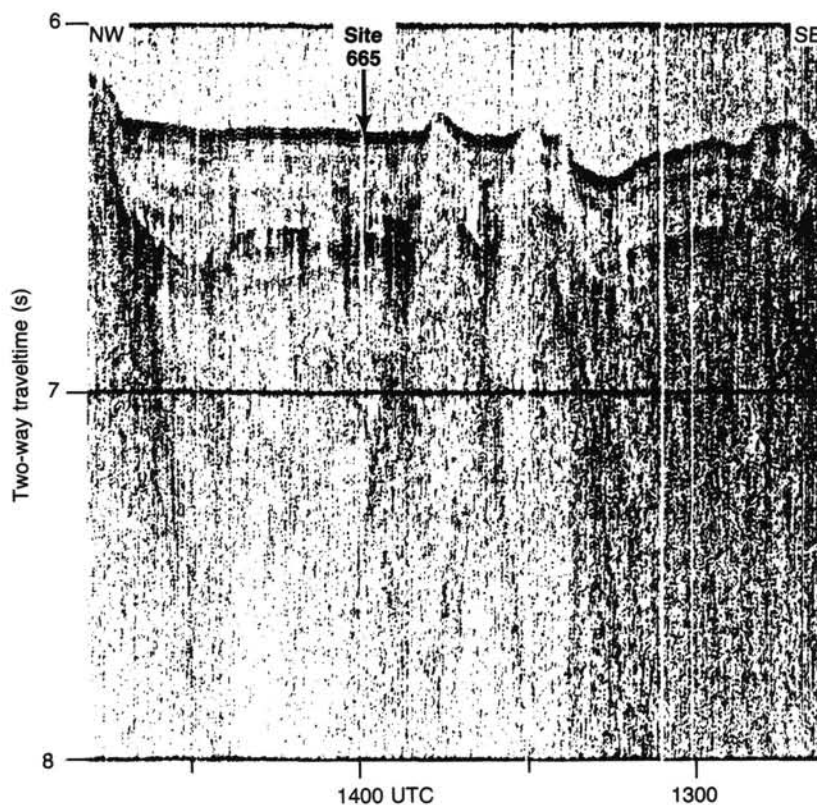


Figure 4. Seismic-reflection record from cruise V2206 (5/18/66) near Site 665.

mus, and *Ceratolithus acutus*). The sequence of ordered biostratigraphic assemblages ends near the disappearance level of *C. acutus*, at the bottom of Section 108-665A-9H-3. The nanofossil preservation at Site 665 is good only in the two first cores (upper Pleistocene), moderate in the lower Pleistocene, and poor in the Pliocene. Severe etching and dissolution of the placoliths and overgrowths on the discoasters are observed in the Pliocene assemblages, although many lower Pliocene samples show beautifully preserved discoaster assemblages.

Cores 108-665A-1H and -665B-1H show a typical late-Pleistocene assemblage from Zones NN20 and NN21, characterized by the dominance of *gephyrocapsids*. As at Site 664, species diversity is low. The disappearance of *Pseudoemiliania lacunosa* occurs in Section 108-665A-2H-5. The last occurrences of the early-Pleistocene markers *Helicosphaera sellii* and *Calcidiscus macintyreii* were observed in Sections 108-665B-4H-4 and -665A-4H-6.

The last late-Pliocene discoasters, *Discoaster brouweri* and *Discoaster triradiatus*, were recognized in Samples 108-665-5H-4, 30 cm, and -665B-5H-1, 140 cm. The increase in abundance of *D. triradiatus* relative to *D. brouweri* occurs between Samples 108-665A-5H-6, 65 cm, and -665A-5H-6, 90 cm, and between Samples 108-665B-5H-2, 90 cm, and -665B-6H-1, 110 cm. These sections are assigned an age of 2.07 Ma.

The last occurrence (LO) of *Discoaster pentaradiatus*, which marks the top of Zone NN17, occurs in Sections 108-665A-6H-4 and -665B-6H-2. The disappearance of *Discoaster surculus* was observed in Section 108-665A-6H-5, suggesting an age of about 2.45 Ma. The LO of *Discoaster asymmetricus* occurs in Sample 108-665A-6H-7, 65 cm, whereas the disappearance of *Discoaster tamalis* was recognized in Sample 108-665A-7H-1, 80 cm.

The LO of sphenoliths occurs in Section 108-665A-8H-3, and the LO of *Reticulofenestra pseudumbilica* occurs immedi-

ately below in Section 108-665A-8H-4. *Amaurolithus delicatus* is present with *Ceratolithus rugosus* from Samples 108-665A-9H-1, 50 cm through -665A-9H-3, 77 cm. The presence of *C. acutus* in Sample 108-665A-9H-3, 140 cm, indicates an age older than 4.6 Ma for this sample. Sample 108-665A-9H-5, 25 cm, contains *Triquetrorhabdulus rugosus*, *Amaurolithus delicatus*, and *Discoaster quinqueramus*. The latter species is probably reworked, as in Sample 108-665B-9H-1, 145 cm, owing to the presence of a slump. Section 108-665A-9H, CC is barren, whereas Section 108-665B-9H, CC shows only poorly preserved Pliocene and late-Miocene discoasters.

Planktonic Foraminifers

The location of this site places it under warm, tropical surface waters, with no influence of cooler currents or strong upwelling. This is reflected in the foraminifer fauna by the common occurrence of tropical species such as *Globigerinoides trilobus*, *Globigerinoides sacculifer*, *Globigerinoides ruber*, and *Globigerinoides obliquus*. The faunas have, however, been strongly affected by dissolution, limiting abundances to common or few and reducing preservation to moderate or poor in most samples. The lowermost Pliocene (below the top of Core 108-665A-9H and below Core 108-665B-8H) is barren.

The *Globorotalia truncatulinoides* Zone was recognized in Sections 108-665A-1H-3, CC and -665B-1H-3, CC. *Neoglobobulimina dutertrei*, together with *G. trilobus* and *G. ruber*, are common in this zone, while *G. sacculifer* and *Globorotalia inflata* are moderately common. Sections 108-665A-4H and -665A-5H, CC contained neither *G. truncatulinoides* nor *G. obliquus* and, consequently, could not be zoned. Samples 108-665B-4H, CC through -665B-5H-5, 90 cm, belong to the PL6 Zone, but this zone was not identified in Hole 665A. Samples 108-665A-6H-4, 73 cm, -665A-6H, CC, -665A-7H-2, 67 cm, -665B-5H, CC, and -665B-6H, CC belong to Zone PL5. The short PL4 Zone was

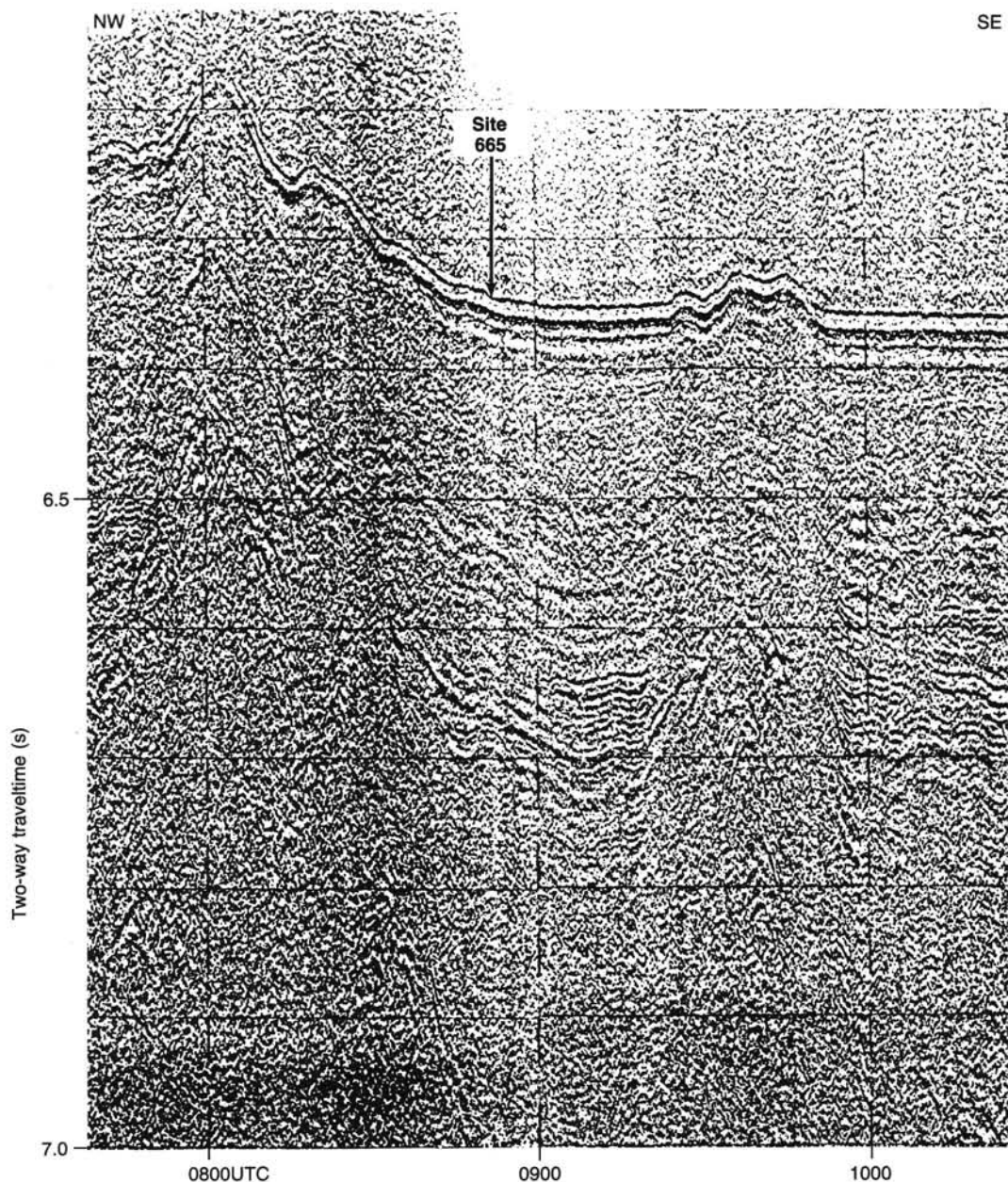


Figure 5. High-resolution, seismic-reflection record near Site 665 from the GEOTROPEX'85 cruise of the *Polarstern* (10/18/85).

recognized only in Sample 108-665A-7H-4, 80 cm, from Hole 665A. In both holes, the PL3 Zone extends to the deepest samples containing foraminifers, Samples 108-665A-9H-1, 57 cm, and -665B-7H, CC. Zones PL3 and PL4 contain common *Globorotalia menardii*, but this species is absent in Zones PL5 and PL6, and rare in the Pleistocene. *Globorotalia inflata* and *Globorotalia puncticulata* are virtually absent in the Pliocene.

Benthic Foraminifers

Benthic foraminifers occur in core-catcher Samples 108-665A-1H through -665A-8H. Except for the lack of uvigerinids, the benthic-foraminifer assemblage is similar in composition to that observed at other Leg 108 sites.

Few-to-rare benthic foraminifers occur in core-catcher Samples 108-665A-1H through -665A-4H. Preservation of specimens is poor to moderate. Sections 108-665A-5H, CC through -665A-

7H, CC (late Pliocene) are characterized by high diversity and common, well-preserved specimens, but the abundant species are different in each sample. In Section 108-665A-5H, CC, *Epistominella exigua* and *Oridorsalis tener* are the dominant species. In Section 108-665A-6H, CC, *Gyroidinoides soldanii*, *Pullenia bulloides*, and *Virgulina texturata* are common. *Globocassidulina subglobosa*, *O. tener*, and *Epistominella umbonifera* are dominant in Section 108-665A-7H, CC. Modern specimens of *E. umbonifera* are considered indicators of Antarctic Bottom Water (AABW), and the other species mentioned are associated with North Atlantic Deep Water (NADW) (Lohmann, 1978). *Globocassidulina subglobosa* is also a marker for warm AABW in the Indian Ocean (Corliss, 1979). The occurrence of these species in Section 108-665A-7H, CC suggests that both NADW and AABW were prevalent during the late Pliocene in the region of Site 665.

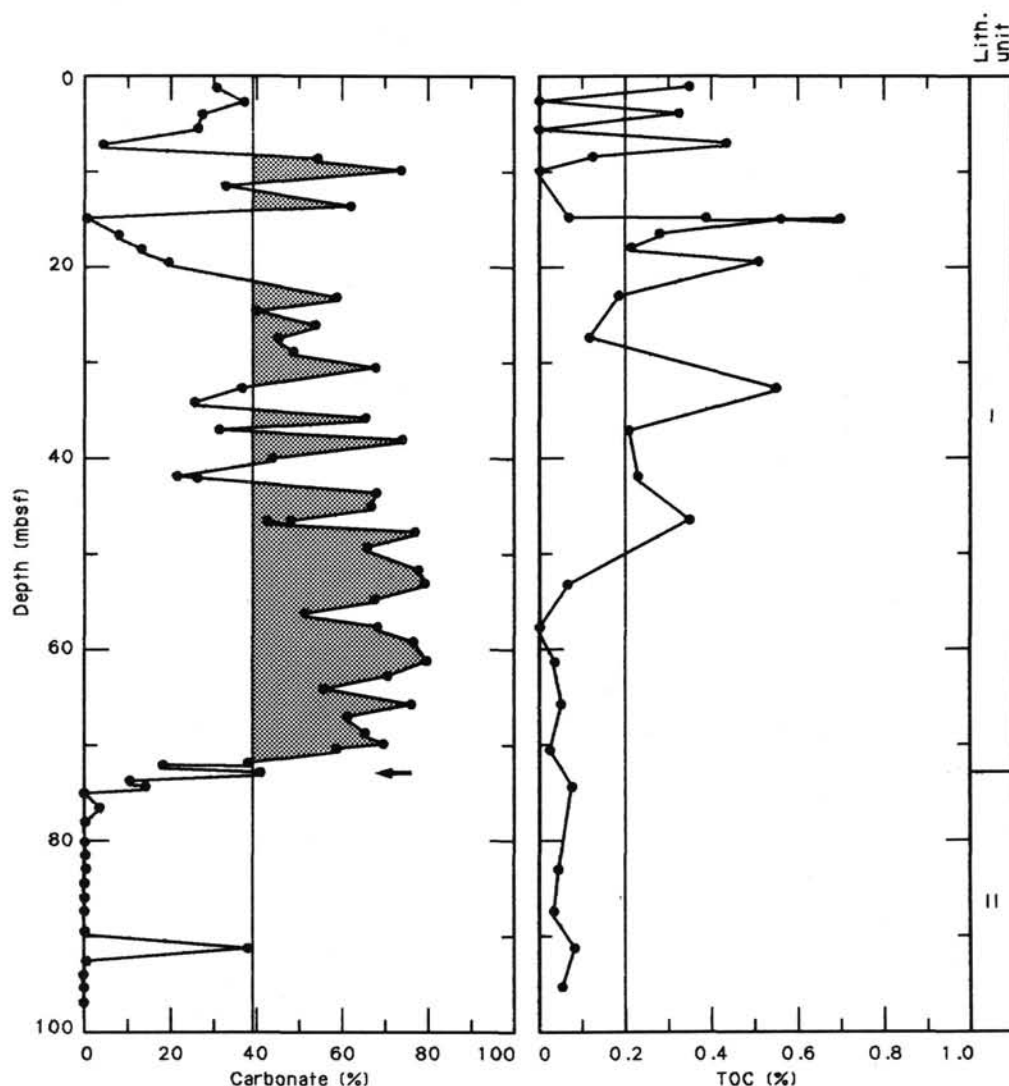


Figure 6. Percentage of carbonate and organic-carbon values vs. depths below seafloor for Site 665A.

Diatoms

All core-catcher samples from Holes 665A and 665B were examined for diatoms. Although rare, poorly preserved specimens were observed in several samples, age-diagnostic species were observed only in Sections 108-665A-2H, CC and -665B-1H, CC, and 108-665B-2H, CC. The occurrence of *Pseudoeunotia doliolus* without *Nitzschia reinholdii* suggests placement of core-catcher Samples 108-665B-1H and -665B-2H in the *Pseudoeunotia doliolus* Zone. The co-occurrence of these species in Section 108-665A-2H, CC assigns this sample to the *Nitzschia reinholdii* Zone.

Rare specimens of either freshwater *Melosira* spp. or *Ethmodiscus rex* occur in core-catcher Samples 108-665A-1H, -665A-4H, -665A-11H, -665B-3H, and -665B-4H. Diatoms were not observed in the remaining core-catcher samples (108-665A-5H, -665A-6H through -665A-10H, -665B-6H, -665B-7H, and -665B-9H).

Note that by examining only core-catcher samples from this site, we have a biased view as to abundance and, therefore, the potential usefulness of the diatoms. Although examination of core-catcher samples suggests an extremely limited occurrence of diatoms in Holes 665A and 665B, diatoms compose 5% to 30% of the sediment in smear slides from some intervals, sug-

gesting greater fluctuations in primary productivity. Samples will be taken from these intervals for onshore analyses.

PALEOMAGNETISM

Magnetostratigraphy

Paleomagnetic results from Site 665 were an unqualified success. Whole-core measurements provided the basis for a high-resolution magnetostratigraphy in sediments too weakly magnetized to measure using discrete-sampling techniques. The core-orientation system, critical for further equatorial drilling, was shown to work well.

Measurements for the archive halves of Cores 108-665A-1H through -665A-9H and 108-665B-1H through -665B-8H were performed at 3-cm intervals. Data from demagnetization to 50 Oe are plotted in Figures 9 and 10. An orientation correction was applied to each core to adjust the mean-normal direction to 90° and the mean-reversed direction to 270°. This was done by first plotting the uncorrected data for each core and then interpreting the record in terms of polarity. Polarity assignments were based primarily on pattern recognition but are supported by magnetic behavior, photographic orientation data from Hole 665B cores, and biostratigraphic zonations.

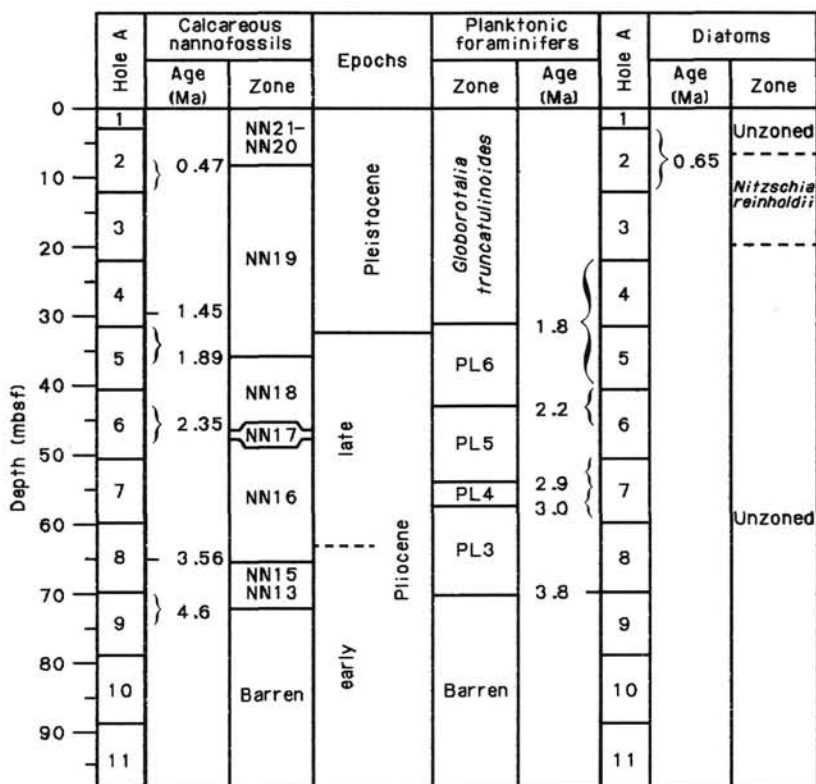


Figure 7. Zonal assignments for cores recovered from Hole 665A.

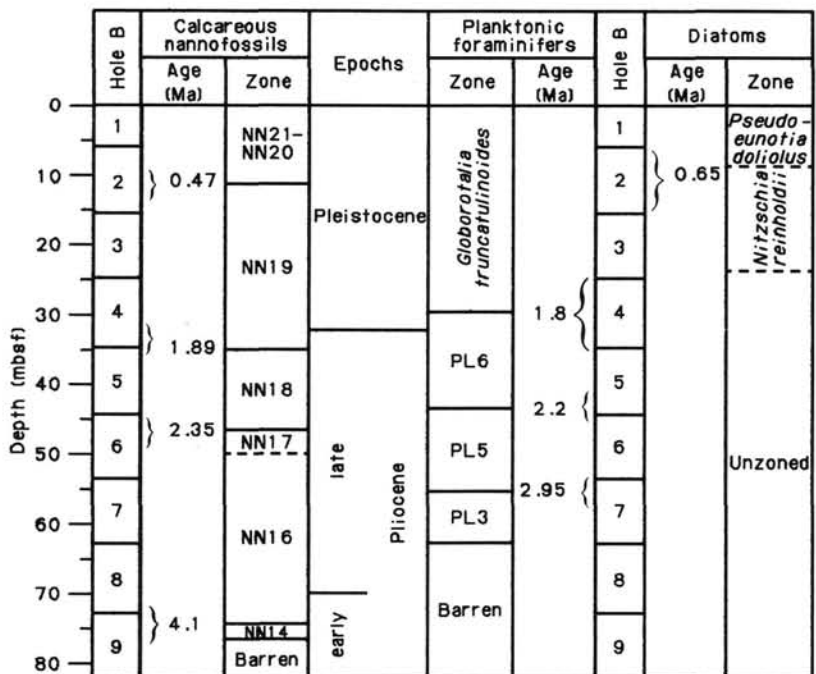


Figure 8. Zonal assignments for cores recovered from Hole 665B.

Magnetic behavior can give clues to polarity by assuming that reversed directions are more likely to be affected by viscous overprinting than are normal ones. Removal of normal overprinting of viscous origin results in an increase in intensity during early demagnetization. We illustrate the difference in behavior in Figure 11. The data shown in Figure 11A is typical of

“normal” samples at this site, displaying a smooth decay to the origin. “Reversed” behavior is shown in Figure 11C and 11D, which have more complicated demagnetization paths.

Cores 108-665B-2H through -665B-7H were oriented using the multishot-photographic orientation system. A compilation of all orientation attempts is given in Table 2. The great discrep-

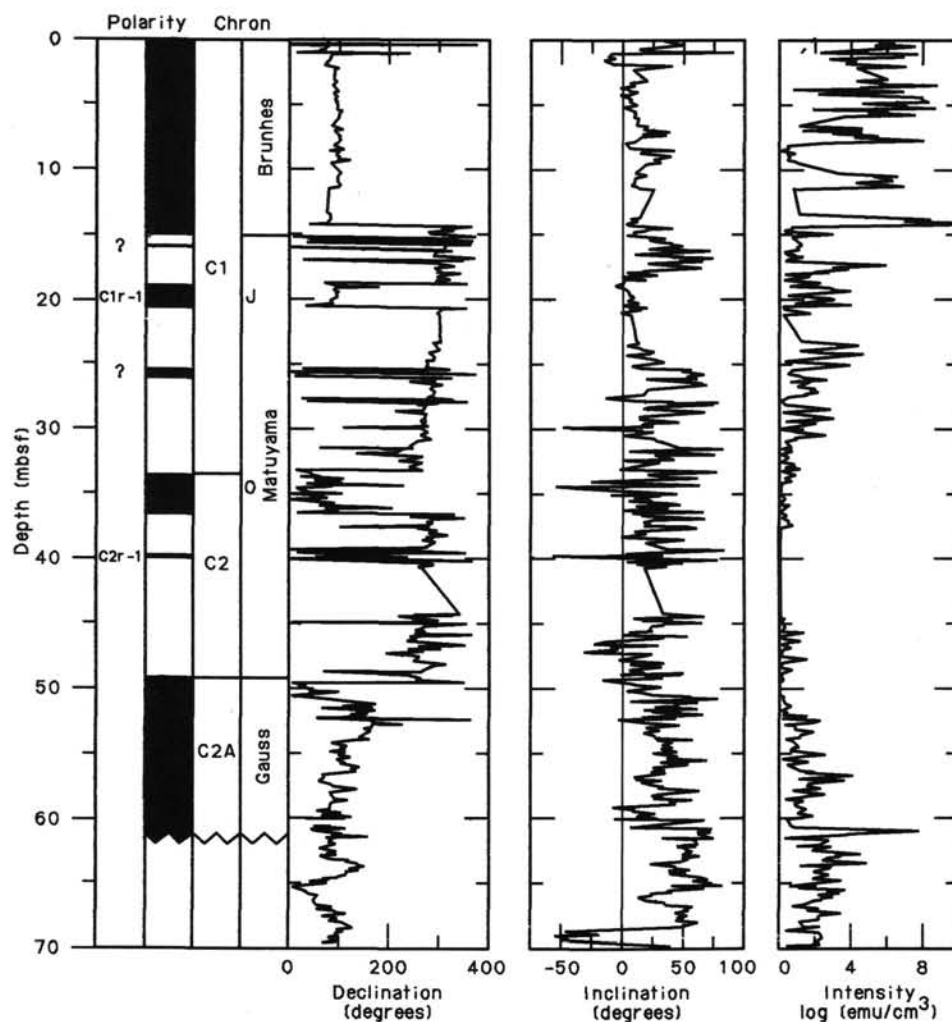


Figure 9. Paleomagnetic data from Hole 665A archive halves demagnetized to 50 Oe. Measurements performed at 3-cm intervals. Declination adjusted so that 90° is normal and 270° is reversed. Polarity intervals greater than 40 cm thick are indicated in polarity log and correlated to the time scale. Intensities are in 10^{-6} emu per volume. Units labeled mystery (MYST) have not been correlated to the time scale.

ancy for Core 108-665B-7H is most likely caused by a strong magnetic overprinting that has disturbed the paleomagnetic declination data. The otherwise excellent agreement supports our interpretation of the polarity of paleomagnetic data from Hole 665B, shown in Figure 10. The correspondence between data from Hole 665A (Table 2) and those from Hole 665B (Table 3) supports our interpretation of polarities from Hole 665A.

So as not to be misled by the illusion of detail given by a 3-cm measuring interval, we have drawn the polarity log by constraining each polarity unit to span at least 40 cm. At a 2 cm/k.y. sediment-accumulation rate, this results in a 20,000-yr resolution, sufficient to establish the magnetostratigraphic pattern, while eliminating instrumental and physical noise. Correlation to the time scale is in excellent agreement with the biostratigraphic zonation, lending further credence to our polarity interpretations.

Depths to reversal boundaries are given in Table 3. Note that, based on correlations facilitated by the *P*-wave-velocity data, mystery unit A-2 and mystery unit B-1 do not record the same polarity subchron. These small polarity units may be either the result of persistent overprinting or one of several short sub-

chrons known from C1r, i.e., the Cobb Mountain or the Vrica subchrons. Both Reunion subchrons (C2r-1 and C2r-2) may occur at Site 665. However, our rather strict rule of a 40-cm thickness has obscured the detail. Further refinement would require subsampling and careful demagnetization.

Intensity records from both holes are shown in Figure 12. Solid lines indicate correlations based on reversal stratigraphy, as discussed before. Intensity records are similar for both holes, with high intensities at the top, much lower intensities in the middle, and higher values at the bottom. Note that intensities less than about 2 on the scale shown in Figure 12 cannot be measured as discrete samples using our shipboard equipment. This threshold is reached at about 30 m in both holes. Therefore, whole-core measurements are essential for providing magnetostratigraphy at this site from 30 to 60 mbsf. Also note that a sampling density of one per 10 cm would be necessary to delineate the magnetostratigraphy. Obtaining and measuring so many samples on board ship or even later would be impossible.

The increased intensity at the bottoms of the holes is caused by a strong, near-vertical, magnetic overprinting characteristic of the red clays. Demagnetization with alternating fields of dis-

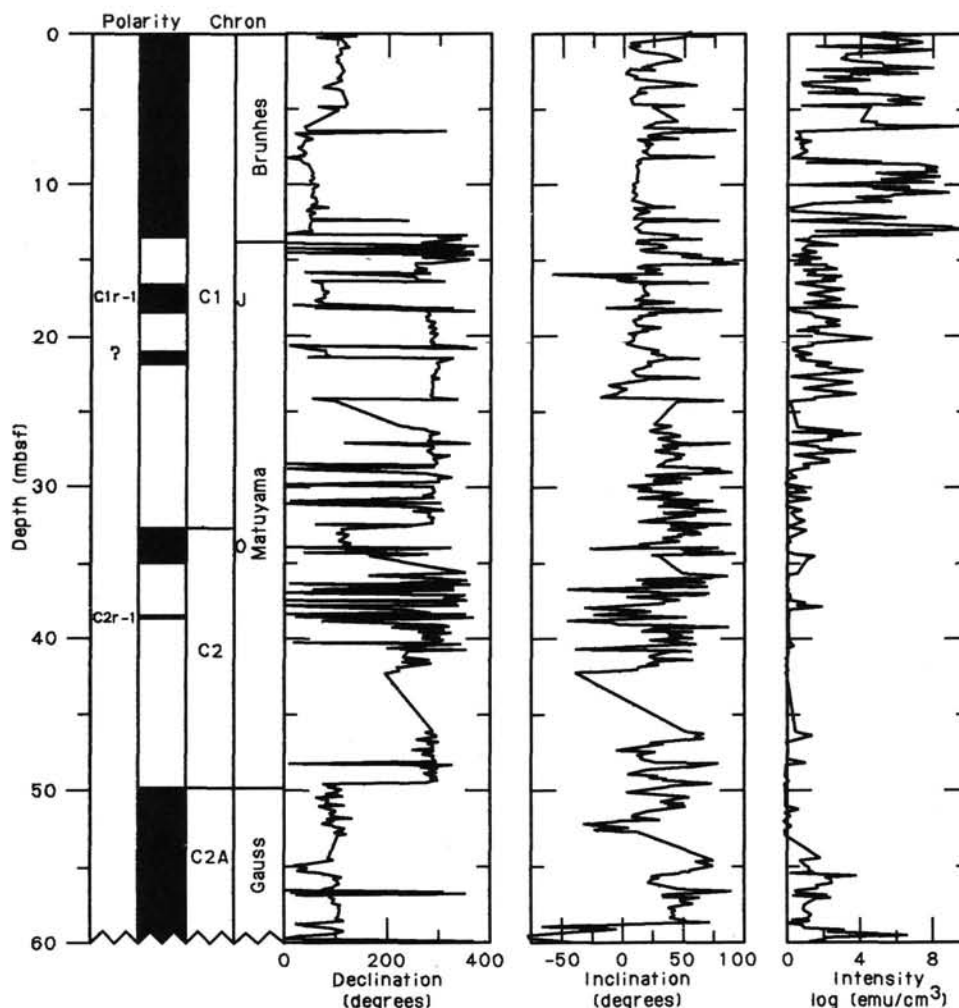


Figure 10. Paleomagnetic data from Hole 665B archive halves demagnetized to 50 Oe. Measurements performed at 3-cm intervals. Declination adjusted so that 90° is normal and 270° is reversed. Polarity intervals greater than 40 cm thick are indicated in polarity log and correlated to the time scale. Intensities are in 10^{-6} emu per volume. Units labeled mystery (MYST) have not been correlated to the time scale.

crete samples revealed no stable component, and thermal demagnetization in a carefully shielded environment will be attempted as part of our shore-based investigation.

Magnetic Susceptibility

At Site 665 the whole-core volume susceptibility records exhibit a pattern of high-frequency variations, with values in the range of 10 to 200×10^{-6} SI units in the microfossil oozes of early Pliocene to Holocene age (lithologic Unit I, 0 to about 70 mbsf in Holes 665A and 665B). The lower Pliocene red clays (lithologic Unit II, about 70 mbsf and below in both holes) have values up to about 1000×10^{-6} SI units. Excellent between-hole correlation of susceptibility features is possible (see Fig. 13) and was used to construct composite-depth sections (see "Composite-Depth Section," this chapter).

SEDIMENT-ACCUMULATION RATES

Sediment-accumulation rates were calculated for Hole 665A based on 13 biostratigraphic events and eight paleomagnetic events (Table 4). Results are plotted in Figure 14. We did not use the LO of the planktonic foraminifer, *Globigerinoides obliquus*, because this datum has, in most cases, proved unreliable at pre-

vious sites. The diatom assemblage was generally sparse in the core-catcher sample examined, precluding the inclusion of diatom datums. Accumulation rates change relatively little throughout the Pleistocene and late Pliocene at Site 665, but are significantly lower in the early Pliocene. The accumulation rate averages ~ 22 m/m.y. in the Pleistocene, decreasing to ~ 15 m/m.y. in the late Pliocene. Minor variations in accumulation rates around 2.2 Ma may be real or may reflect the presence of a slump or turbidite. Distorted bedding between 40 and 45 mbsf favors the latter explanation.

Accumulation rates are substantially lower before 3.6 Ma, but the exact timing of this change in rate remains ambiguous. Identification of the LO of *Globigerina nepenthes* (3.9 Ma) could help resolve this issue, but the lower Pliocene sediment consists of red clay barren of planktonic foraminifers below 70 mbsf. The carbonate-rich sample (108-665A-9H, 56–58 cm) just above the top of the red-clay facies did not contain *G. nepenthes*, and, thus, the top of this unit should be younger than 3.9 Ma. Assuming the increase in accumulation rates correlates with the transition from red-clay to more carbonate-rich facies, the top of the clay unit has an estimated age of ~ 3.8 Ma, and the sedimentation rate of the clay unit is ~ 4 m/m.y.

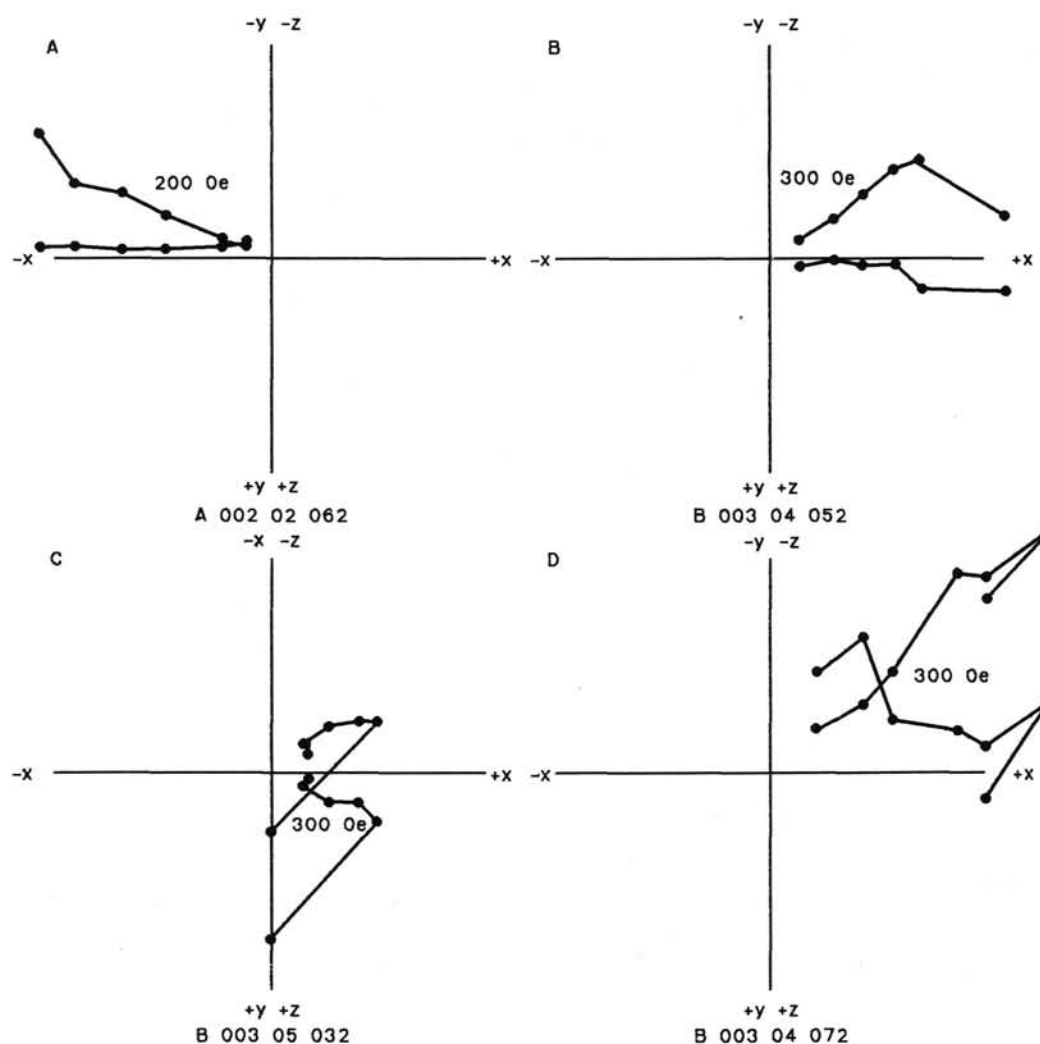


Figure 11. Demagnetization data from discrete samples. Crosses indicate the horizontal projection of the magnetic vector; circles indicate vertical projection. Data were not corrected for declination.

INORGANIC GEOCHEMISTRY

Interstitial-water samples were squeezed from two sediment samples routinely taken approximately every 50 m from Hole 665A. Values for pH and alkalinity were measured in conjunction, using a Metrohm 605 pH-meter, followed by titration with 0.1N HCl, and salinities were measured using an optical refractometer. Cl^- , Ca^{2+} , and Mg^{2+} concentrations were determined by the titrations described in Gieskes and Peretsman (1986). SO_4^{2-} analyses were conducted by ion chromatography using a Dionex 2120i instrument. Results from all analyses are presented in Table 5.

ORGANIC GEOCHEMISTRY

At Site 665, Hole 665A, the carbonate contents of 71 physical-property and smear-slide samples were determined. Of these, 30 samples from throughout the sequence also were analyzed for total-organic-carbon (TOC) contents. Eleven samples were investigated for organic-matter type by Rock-Eval pyrolysis. No analyses were performed on samples from Hole 665B.

Organic and Inorganic Carbon

Inorganic-carbon (IC) contents were measured using the Coulometrics Carbon Dioxide Coulometer, while total-carbon (TC)

values were determined using the Perkin Elmer 240C Elemental Analyzer. TOC values were calculated by difference. Analytical methods are discussed, and data listed in the Appendix (this volume).

The TOC contents determined for Hole 665A are generally low, fluctuating between 0.0% and 0.7%, with the highest values lying within the upper 50 m of the sequence. According to Rock-Eval data, the organic matter probably is mainly marine in origin, with two exceptions: in Sections 108-665A-2H-1 and -665A-3H-5 terrigenous organic matter is dominant (Fig. 15 and Table 6). Below around 50 m, all analyzed samples contain less than 0.1% organic carbon. The highest recorded organic-carbon content of 0.7% in Core 108-665A-3H corresponds to a thin layer of diatom ooze (see "Lithostratigraphy and Sedimentology" section, this chapter).

According to carbonate content, the sediment sequence at Site 665 may be divided into two distinct parts (Fig. 15), corresponding to lithologic Units I and II (see "Lithostratigraphy and Sedimentology" section, this chapter). The boundary between these two units lies within Section 108-665A-9H-3 (about 73 mbsf; about 3.8 Ma; see "Sediment-Accumulation Rates" section, this chapter). Unit I is characterized by quasiperiodic variations in carbonate content between 0% and 80%, with most samples lying within the 20% to 80% range. The lowest values are found in the upper 20 m and correspond to levels of diatom

Table 2. Comparison of photographic orientation (MS) with paleomagnetic declination (PMAG).

Site/core	MS	PMAG	Difference (P + M) ^a	Comments
659A-3H	57-58	310	7	
659A-4H	230-237	143	13	
659A-5H	70-72	303	13	
659A-8H	149-150	206	355	
659A-9H				Film ran out
659A-14H-17H				Electronic failure
659B-3H	128			Core not recovered
664C-3H	193	200	33	
664C-4H	13			Set pin sheared
664C-5H	349	49	38	
664C-6H	150	240	30	
664D-3H	0	20	20	
664D-4H	162	227	29	
664D-5H-6H				Blank film
665B-2H	270	90	0	
665B-3H	207	160	7	
665B-4H	100	260	0	
665B-5H	329	30	359	
665B-6H	290	30	320	
665B-7H	225	10	235	
665B-8H				Core not recovered
665B-9H				Core disturbed

^a The difference (P + M) represents the discrepancy between MS and PMAG.

Table 3. Depths to reversal boundaries for Site 665A.

Boundary/ chron	Depth A (mbsf)	Depth B (mbsf)	Age (Ma)
Brunhes/Matuyama (C1/C1r)	14.75	13.75	0.73
upper Jaramillo (C1r-1y)	19.25	16.90	0.91
lower Jaramillo (C1r-1o)	20.95	18.75	0.98
upper Olduvai (C2y)	33.15	32.55	1.66
lower Olduvai (C2o)	36.35	34.3-35.0	1.88
Reunion (C2r-1)	39.80	38.40	2.??
Matuyama/Gauss (C2r/C2A)	49.10	49.10	2.47

ooze. Unit II is almost devoid of carbonate, with values generally ranging between 0% and 1% (Fig. 15). The anomalously high carbonate content (38.9%) of one sample within Core 108-665A-11H corresponds to a thin layer believed to be a slump (see "Lithostratigraphy and Sedimentology" section, this chapter).

Discussion

The sediments at Site 665 display variable organic-carbon contents ranging between 0.0% and 0.7%. The upper part of the sequence (55 mbsf) contains several levels that are relatively enriched in marine organic carbon (up to 0.7% TOC) and biogenic silica (see "Lithostratigraphy and Sedimentology" section, this chapter), possibly reflecting periods of increased productivity. Below 55 mbsf (i.e., before about 2.8 Ma), organic productivity and/or preservation appears to have been low, as indicated by low organic-carbon contents of <0.1%. Such low organic-carbon contents are typical of open-marine environments (Müller et al., 1983).

The sediments of Unit II contain little or no carbonate, indicating that before about 3.8 Ma, deposition was below the CCD.

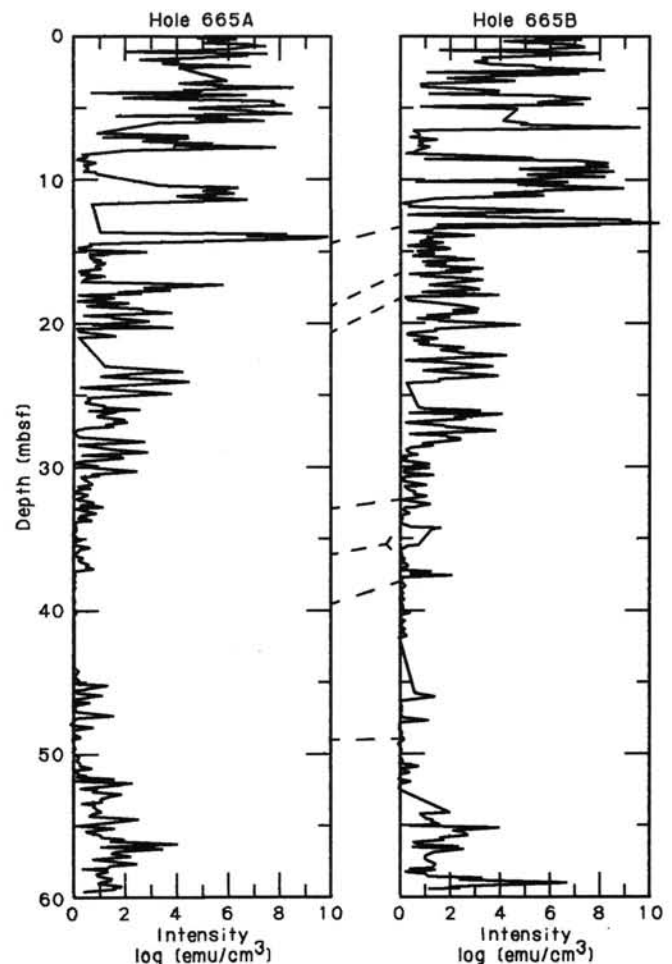


Figure 12. The NRM intensity logs for Holes 665A and 665B. Solid lines indicate magnetostratigraphic correlations between the two holes.

A subsequent change in the position of the CCD resulted in the accumulation of sediments with quasiperiodic variations in carbonate content between 20% and 80%.

PHYSICAL PROPERTIES

The techniques used for shipboard physical-property measurements at Site 665 are outlined in the "Introduction and Explanatory Notes" (this volume). Index-properties and vane-shear-strength measurements were performed on samples from both Holes 665A and 665B. These data are shown in Tables 7 through 9 and in Figures 16 through 22. Profiles of the calcium carbonate content and grain density for Hole 665A are shown in Figure 19. The P-wave-logger profile for Hole 665A is shown in Figure 22. No data presented here were screened for bad data points.

The wet-bulk density (Figs. 16 and 19) increases from about 1.2 g/cm³ at the mud line to about 1.55 g/cm³ at a depth of 75 mbsf, as the average carbonate content increases from an average value of 30% to 70%. Below this, the carbonate content decreases rapidly to near 0%. This is reflected by a decrease in the wet-bulk density to below 1.4 g/cm³ within this clay unit. Other index properties show similarly related trends. The vane shear strength increases rapidly in the clay from about 20 kPa at 60 mbsf to about 100 kPa at 95 mbsf (Fig. 21).

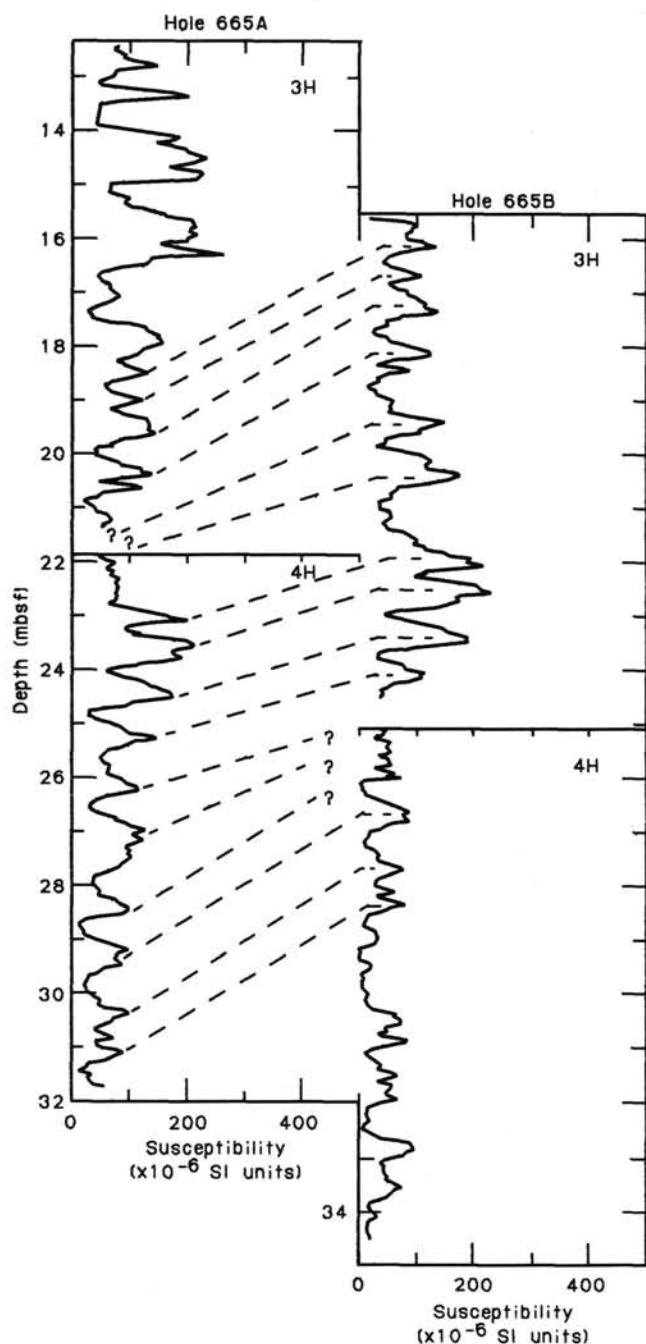


Figure 13. Examples of magnetic-susceptibility correlations between Holes 665A and 665B.

SEISMIC STRATIGRAPHY

At Site 665, the deepest Hole (665A) was drilled only to a depth of 97.9 mbsf, and Hole 665B was drilled only to 82.0 mbsf. Water-gun seismic profiler records obtained during our approach to Site 665 indicate three seismic units (Fig. 23) within the narrow range of the seismic record equivalent to the cored interval:

Seismic unit 1, 0–0.05 s, is an upper unit with a false acoustic signal caused by the water guns. This unit should equate to about the upper 38 m of sediment.

Seismic unit 2, 0.05–0.10 s, is a middle unit, with two major reflectors and a series of thin, faint reflectors between the major

Table 4. Biostratigraphic and magnetostratigraphic datums used to construct an age-depth plot for Site 665A.

Datum	Depth (mbsf)	Age (Ma)
LO <i>Pseudoemiliana lacunosa</i>	8.9–9.5	0.47
Brunhes/Matuyama	14.8–14.8	0.73
Matuyama/Jaramillo	19.3–19.3	0.91
Jaramillo/Matuyama	21.0–21.0	0.99
LO <i>Calcidiscus macintyreii</i>	29.9–30.7	1.45
Matuyama/Olduvai	33.2–33.2	1.66
Olduvai/Matuyama	36.4–36.4	1.88
LO <i>Discoaster brouweri</i>	35.6–36.8	1.89
Reunion (upper)	39.4–39.4	2.03
FO <i>Discoaster triradiatus acme</i>	39.6–39.8	2.07
Reunion (lower)	39.8–39.8	2.13
LO <i>Globorotalia miocenica</i>	40.9–46.1	2.20
LO <i>Discoaster pentaradiatus</i>	45.5–47.0	2.35
LO <i>D. surculus</i>	47.0–48.5	2.45
Matuyama/Gauss	49.1–49.1	2.47
LO <i>Discoaster tamalis</i>	50.7–51.2	2.65
LO <i>Dentoglobobadrina altispira</i>	52.6–55.7	2.90
LO <i>Sphaeroidinellopsis semulina</i>	55.7–58.9	3.00
LO <i>Sphenolithus abies</i>	63.8–64.4	3.45
LO <i>Reticulofenestra pseudoumbilica</i>	65.0–65.4	3.56
FO/LO <i>Ceratolithus rugosus/C. actutus</i>	72.7–73.8	4.60

LO = last occurrence. FO = first occurrence.

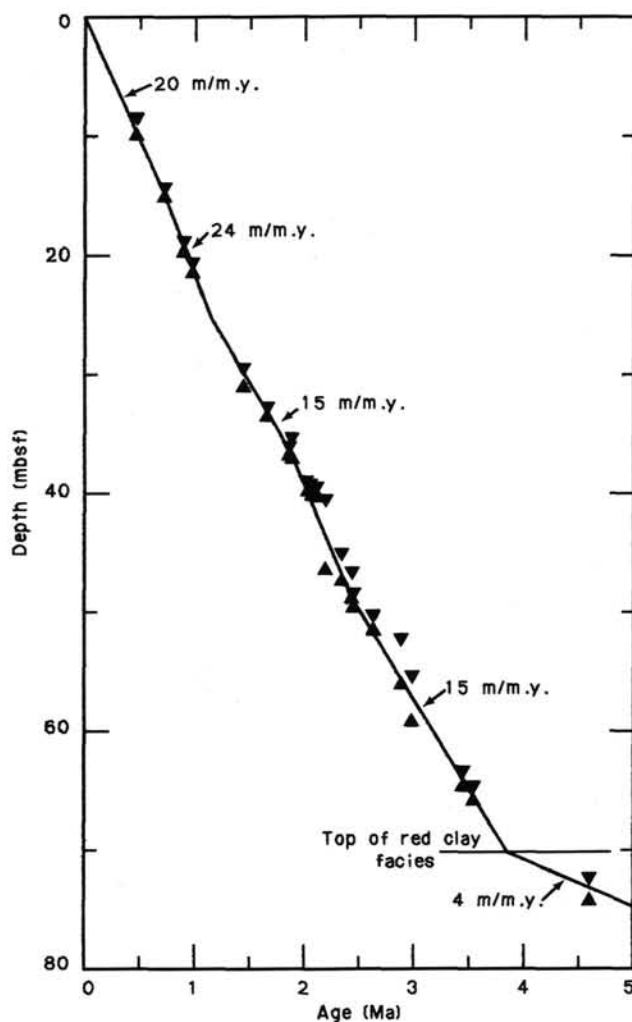


Figure 14. Sediment-accumulation rates for Site 665, Hole 665A.

Table 5. Results of organic-geochemical analyses conducted for Site 665.

Core/ section	pH	Alkalinity (mmol/L)	Salinity (‰)	Chlorinity (mmol/L)	SO ₄ ²⁻ (mmol/L)	Mg ²⁺ (mmol/L)	Ca ²⁺ (mmol/L)
1-1	7.62	3.29	34.2	567.0	18.08	52.22	10.95
6-5	7.72	4.25	34.5	580.0	16.90	50.05	12.96

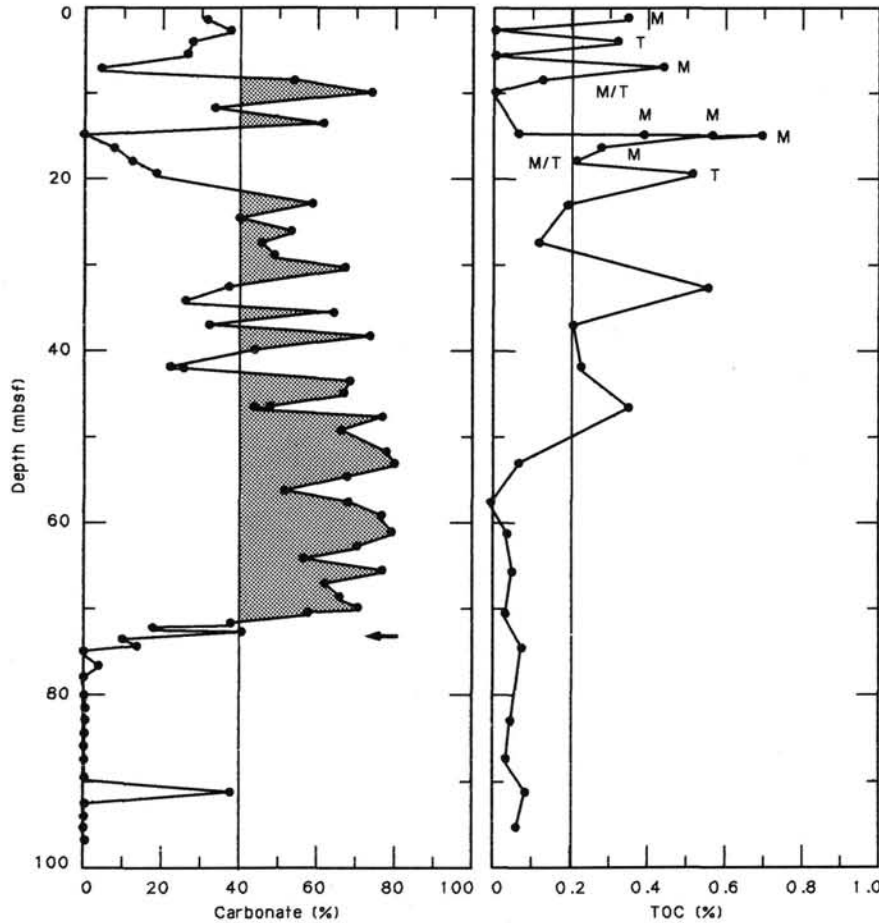


Figure 15. Carbonate and total-organic-carbon records for Site 665, Hole 665A. The arrow marks the division between lithologic Units I and II. *M* = dominant marine, *M/T* = mixed, and *T* = dominant terrigenous organic matter (data based on Rock-Eval pyrolysis; Table 6).

units. This unit should equate to the interval of about 38 to 76 mbsf in the sediment section.

Seismic unit 3, 0.10–>0.20 s, is a lower unit with well-developed, evenly spaced reflectors of moderate strength. This unit should equate to the interval below 76 mbsf in the sediment column.

We used a mean sound velocity of 760 m/s for the entire sediment section at Site 665 (see “Physical Properties” section, this chapter) to evaluate possible correlations of both seismic lithologic units (Fig. 23). Seismic unit 1 is an artifact. Seismic unit 2 roughly corresponds to the lower one-half of lithologic Unit I, which consists of Pliocene–Pleistocene calcareous ooze cycles from 0 to 70 mbsf (Fig. 23). The top of seismic unit 3 corresponds to the early Pliocene (and older) red-clay facies encountered below 70 mbsf.

COMPOSITE-DEPTH SECTION

At Site 665, the magnetic-susceptibility signal returned to intensity levels strong enough to be useful for between-hole corre-

lations and for construction of a composite-depth section (Tables 10 and 11). This technique provided correlations to as deep as 65–68 mbsf in Cores 108-665A-8H and -665B-7H. No recovery was possible for Core 108-665B-8H, thus ending the correlation sequence. Table 10 shows a correlation scheme in which Hole 665A is the primary record, and Hole 665B provides short sequences to connect core breaks in Hole 665A. Table 11 uses Hole 665B as the primary record.

The correlated sequences span almost the entire upper-Pliocene and Holocene sequence of nannofossil and clay-bearing oozes. The continuous composite-depth sequence thus spans the last 3.5 to 4.0 Ma of late Neogene time. The only uncertain correlation is between Cores 108-665A-6H and -665B-5H, at an age of about 2.4 Ma.

REFERENCES

Corliss, B. H., 1979. Taxonomy of recent deep-sea benthonic foraminifera from the southern Indian Ocean. *Micropaleontol.*, 25:1–19.
 Curry, W. B., and Lohmann, G. P., 1983. Reduced advection into Atlantic Ocean deep eastern basins during last glaciation maximum. *Nature*, 306:577–580.

- Curry, W. B., and Lohmann, G. P., 1984. Carbon deposition rates and deep water residence time in the equatorial Atlantic Ocean throughout the last 160,000 years. *Am. Geo. Union Chapman Conf. on Natural Variations in Carbon Dioxide and the Carbon Cycle*, 285-301.
- Gieskes, J. M., and Peretsman, G., 1986. Water chemistry procedures aboard the *JOIDES Resolution*. ODP Technical Report No. 5.
- Jacobi, R. D., and Hayes, D. E., 1982. Bathymetry, microphysiography, and reflectivity characteristics of the west African margin between Sierra Leone and Mauritania. In von Rad, U., et al. (Eds.), *Geology of the Continental Margin*: New York (Springer-Verlag), 182-212.
- Lohmann, G. P., 1978. Abyssal benthonic foraminifera as hydrographic indicators in the western South Atlantic Ocean. *J. Foram. Res.*, 8:6-34.
- Müller, P., Erlenkeuser, H., and von Grafenstein, R., 1983. Glacial-interglacial cycles in oceanic productivity inferred from organic carbon contents in eastern North Atlantic sediment cores. In Thiede, J., and Suess, E. (Eds.), *Coastal Upwelling: Its Sediment Record*, Part B: New York (Plenum Press), 365-398.

Table 6. Results of Rock-Eval pyrolysis for Site 665.

Sample (cm)	TOC (%)	HI	OI	C _{org}
1-1, 120	0.35	677	2122	^a M
2-1, 120	0.33	121	1700	^b T
2-3, 120	0.44	1047	691	M
2-4, 120	0.57	933	347	M
3-2, 111	0.39	1172	443	M
3-2, 116	0.70	1309	247	M
3-2, 120	0.57	933	347	M
3-3, 119	0.28	993	457	M
3-4, 119	0.21	433	2148	^c M/T
3-5, 120	0.52	46	900	T
6-1, 93	0.23	326	2430	M/T

^a M = dominant marine.

^b T = dominant terrigenous organic matter.

^c M/T = mixed marine and terrigenous.

Note: TOC = total organic carbon; HI = hydrogen index; and OI = oxygen index.

Table 7. Index-properties and vane-shear-strength data for Hole 665A.

Core/section	Interval (cm)	Depth (mbsf)	Gain Density (g/cm ³)	Wet-water content (%)	Dry-water content (%)	Wet-bulk density (g/cm ³)	Dry-bulk density (g/cm ³)	Porosity (%)	Vane shear strength (kPa)
108-665A-1-1	121	1.21	2.54	68.34	215.87	1.26	0.44	84.59	4.00
108-665A-1-2	121	2.71	2.62	68.36	216.03	1.26	0.44	84.96	4.00
108-665A-2-1	121	4.11	2.50	64.31	180.16	1.29	0.50	81.78	2.80
108-665A-2-2	121	5.61	2.56	60.90	155.75	1.33	0.56	79.90	6.00
108-665A-2-3	121	7.11	2.77	70.80	242.42	1.25	0.40	87.06	4.20
108-665A-2-4	121	8.61	2.58	58.42	140.48	1.36	0.62	78.26	1.60
108-665A-2-6	121	11.31	2.52	62.52	166.84	1.31	0.54	80.70	6.60
108-665A-3-1	121	13.44	2.63	59.30	145.73	1.36	0.60	79.19	15.00
108-665A-3-2	121	14.92	2.47	77.64	347.27	1.17	0.30	89.65	14.00
108-665A-3-3	121	16.42	2.43	69.61	229.02	1.24	0.42	84.78	14.60
108-665A-3-4	121	17.92	2.44	61.89	162.40	1.31	0.50	79.81	16.40
108-665A-3-5	121	19.42	1.90	76.47	325.08	1.14	0.31	86.26	32.00
108-665A-3-6	121	20.92	2.68	54.83	121.39	1.42	0.67	76.36	23.00
108-665A-4-1	121	23.11	2.56	54.72	120.87	1.40	0.67	75.41	20.00
108-665A-4-2	121	24.53	2.53	56.80	131.46	1.37	0.64	76.75	21.00
108-665A-4-3	121	26.03	2.51	56.47	129.74	1.38	0.64	76.41	24.00
108-665A-4-4	121	27.53	2.46	57.83	137.12	1.35	0.62	77.03	20.00
108-665A-4-5	121	29.03	2.57	57.26	133.97	1.37	0.63	77.38	30.00
108-665A-4-6	121	30.53	2.58	48.77	95.21	1.48	0.80	70.84	28.00
108-665A-5-1	121	32.61	2.55	56.44	140.61	1.36	0.61	78.12	28.00
108-665A-5-2	121	34.11	2.57	59.01	143.98	1.35	0.59	78.61	29.00
108-665A-5-3	121	35.61	2.61	51.01	104.12	1.45	0.76	72.92	38.00
108-665A-5-4	121	37.11	2.58	52.33	109.78	1.43	0.72	73.73	39.00
108-665A-5-5	81	38.21	2.61	47.60	90.85	1.50	0.82	70.13	41.00
108-665A-5-6	121	39.81	2.49	52.98	112.66	1.41	0.71	73.60	33.00
108-665A-6-1	101	41.85	2.34	56.34	129.06	1.35	0.64	75.04	24.00
108-665A-6-2	121	43.50	2.52	46.03	85.27	1.50	0.85	68.02	24.00
108-665A-6-3	121	45.00	2.67	46.05	85.37	1.53	0.86	69.29	26.00
108-665A-6-4	121	46.50	2.55	49.79	99.17	1.46	0.77	71.50	36.00
108-665A-6-5	121	46.00	2.59	47.63	90.94	1.49	0.83	70.01	22.00
108-665A-6-6	101	49.30	2.58	45.52	83.56	1.52	0.89	68.05	23.00
108-665A-7-1	121	51.61	2.54	44.74	80.96	1.52	0.88	67.02	34.00
108-665A-7-2	121	53.05	2.77	46.12	85.59	1.55	0.88	70.11	37.00
108-665A-7-3	121	54.55	2.60	46.15	85.71	1.52	0.86	68.78	37.00
108-665A-7-4	121	56.05	2.60	43.80	77.92	1.55	0.93	66.68	33.00
108-665A-7-5	121	57.55	1.91	44.47	80.10	1.38	0.89	60.34	30.00
108-665A-7-6	121	59.05	2.38	43.03	75.52	1.51	0.94	64.02	23.00
108-665A-8-1	121	61.11	2.52	40.81	68.93	1.58	0.98	63.25	1.00
108-665A-8-2	121	62.61	2.66	41.65	71.37	1.59	0.98	65.27	21.00
108-665A-8-3	121	64.11	2.29	40.53	68.16	1.52	0.97	60.69	26.00
108-665A-8-4	121	65.61	2.53	42.81	74.86	1.55	0.94	65.20	24.00
108-665A-8-5	101	66.91	2.55	40.92	69.25	1.58	0.98	65.60	29.00
108-665A-8-6	121	68.32	2.49	40.89	69.17	1.57	0.98	63.02	26.00
108-665A-9-1	101	70.41	2.48	40.00	66.68	1.58	1.00	62.02	28.00
108-665A-9-2	121	72.11	2.78	41.74	71.63	1.62	0.97	66.34	50.00
108-665A-9-3	121	73.61	2.69	42.54	74.03	1.59	0.96	66.34	62.00
108-665A-9-4	121	75.11	2.27	42.17	72.91	1.50	0.94	62.07	64.00
108-665A-9-5	121	76.61	2.61	42.72	74.59	1.57	0.95	65.85	70.00
108-665A-9-6	121	78.11	2.59	44.30	79.55	1.54	0.92	67.09	64.00
108-665A-10-1	121	80.07	2.30	50.54	102.18	1.41	0.76	70.03	45.00
108-665A-10-2	121	81.57	2.49	45.13	82.26	1.51	0.89	67.00	71.00
108-665A-10-3	121	83.07	2.47	43.26	76.23	1.53	0.93	65.12	75.00
108-665A-10-4	121	84.57	2.41	48.03	92.41	1.46	0.81	68.78	50.00
108-665A-10-5	121	86.07	2.37	50.97	103.97	1.42	0.74	70.99	40.00
108-665A-10-6	121	87.57	2.55	46.79	87.92	1.50	0.84	68.93	75.00

Table 8. Index-properties and vane-shear-strength data for Hole 665B.

Core/ section	Interval (cm)	Depth (mbsf)	Grain density (g/cm ³)	Wet-water content (%)	Dry-water content (%)	Wet-bulk density (g/cm ³)	Dry-bulk density (g/cm ³)	Porosity (%)	Vane shear strength (kPa)
108-665B-1-1	121	1.21	2.40	68.44	216.82	1.25	0.43	83.88	5.60
108-665B-1-2	121	2.71	2.51	67.29	205.68	1.27	0.46	83.74	4.40
108-665B-1-3	121	4.21	2.33	67.75	210.06	1.25	0.45	83.07	7.00
108-665B-1-4	111	5.61	2.59	67.37	206.51	1.27	0.46	84.22	11.60
108-665B-2-1	121	7.21	2.64	69.69	229.92	1.25	0.42	85.84	15.00
108-665B-2-2	121	8.71	2.55	52.65	111.21	1.43	0.70	73.80	30.00
108-665B-2-3	121	10.21	2.51	64.74	183.63	1.29	0.48	82.12	33.00
108-665B-2-4	121	11.71	2.38	73.46	276.79	1.20	0.36	86.89	26.00
108-665B-2-5	121	13.21	2.41	69.29	225.66	1.24	0.42	84.47	34.00
108-665B-2-6	121	14.71	2.52	63.38	173.04	1.30	0.54	81.27	32.00
108-665B-3-1	121	16.71	2.64	61.81	161.82	1.33	0.55	80.97	19.00
108-665B-3-2	121	18.21	2.72	54.70	120.73	1.42	0.67	76.51	15.00
108-665B-3-3	121	19.71	2.58	54.72	120.85	1.40	0.67	75.60	24.00
108-665B-3-4	121	21.21	2.56	50.48	101.92	1.45	0.76	72.13	28.00
108-665B-3-6	121	24.21	2.62	53.13	113.35	1.43	0.71	74.63	22.00
108-665B-4-1	121	26.21	2.62	50.74	103.00	1.46	0.75	72.80	20.00
108-665B-4-2	121	27.71	2.61	56.80	131.48	1.38	0.63	77.30	20.00
108-665B-4-3	121	29.21	2.59	54.02	117.50	1.41	0.69	75.09	26.00
108-665B-4-4	121	30.71	2.52	53.33	114.26	1.41	0.71	74.05	31.00
108-665B-4-5	121	32.21	2.58	51.60	106.62	1.44	0.74	73.20	26.00
108-665B-4-6	121	33.71	2.46	54.74	120.96	1.39	0.67	74.73	34.00
108-665B-5-1	121	35.71	2.72	45.41	83.17	1.55	0.89	69.08	37.00
108-665B-5-2	121	37.21	2.65	58.32	139.91	1.37	0.60	78.66	31.00
108-665B-5-3	121	38.71	2.60	45.32	82.87	1.53	0.88	68.11	29.00
108-665B-5-4	121	40.21	2.62	52.54	110.72	1.44	0.72	74.24	29.00
108-665B-5-5	121	41.71	2.72	52.21	109.25	1.45	0.74	74.68	39.00
108-665B-6-2	121	46.71	2.54	50.44	101.78	1.45	0.77	71.92	27.00
108-665B-6-3	121	48.21	2.57	43.30	76.37	1.55	0.91	66.04	35.00
108-665B-6-4	121	49.71	2.62	46.20	85.87	1.52	0.85	69.02	36.00
108-665B-6-5	121	51.21	2.65	47.49	90.43	1.51	0.83	70.32	27.00
108-665B-7-1	121	54.65	2.44	47.76	91.43	1.47	0.80	68.87	21.00
108-665B-7-2	121	56.15	2.62	40.91	69.23	1.60	0.98	64.20	26.00
108-665B-7-3	121	57.65	2.75	43.37	76.59	1.58	0.93	67.57	25.00
108-665B-7-4	121	59.15	2.58	40.26	67.39	1.60	0.99	63.19	23.00
108-665B-7-5	121	60.65	2.54	41.31	70.38	1.57	0.96	63.83	20.00
108-665B-9-1	121	73.71	2.55	46.32	86.28	1.51	0.87	68.56	56.00
108-665B-9-2	121	75.21	2.55	46.32	86.28	1.51	0.87	68.56	56.00
108-665B-9-3	121	76.71	2.55	46.32	86.28	1.51	0.87	68.56	62.50
108-665B-9-5	61	77.96	2.57	48.75	95.14	1.48	0.81	70.77	80.00
108-665B-9-6	121	80.06	2.57	48.75	95.14	1.48	0.81	70.77	102.50
108-665B-11-1	121	89.61	2.54	49.96	99.83	1.46	0.76	71.50	90.00
108-665B-11-2	121	91.11	2.70	52.22	109.30	1.45	0.73	74.49	95.00
108-665B-11-3	121	92.61	2.55	52.13	108.88	1.43	0.72	73.37	93.00
108-665B-11-4	121	94.11	2.58	53.24	113.87	1.42	0.70	74.48	93.00
108-665B-11-5	111	95.51	2.53	56.26	128.63	1.38	0.65	76.36	88.00
108-665B-11-6	121	96.81	2.53	61.28	158.25	1.33	0.56	78.81	98.00

Table 9. Synthesis of P-wave-logger velocity data for Hole 665A and thermal-conductivity data for Hole 665B.

Hole 665A				Hole 665B			
Depth (m)	P-wave velocity (km/s)	Depth (m)	P-wave velocity (km/s)	Core/ section	Interval (cm)	Depth (m)	Thermal conductivity (W/m/°C)
1.00	1.525	48.10	1.517	2-2	120	8.70	1.0370
2.00	1.532	49.40	1.527	2-3	120	10.20	0.8970
4.90	1.518	51.40	1.517	2-4	120	11.70	0.8620
6.90	1.522	52.40	1.517	2-5	120	13.20	0.8350
8.20	1.522	53.90	1.510	3-2	120	18.20	0.9790
8.70	1.508	55.40	1.514	3-3	120	19.70	1.0030
9.90	1.520	56.90	1.519	3-4	120	21.20	2.5810
10.70	1.570	58.40	1.522	3-5	120	22.70	0.9290
11.90	1.520	60.90	1.540	3-6	120	24.20	1.0260
13.40	1.540	62.40	1.536	4-2	120	27.70	0.9170
13.80	1.542	63.20	1.560	4-3	120	29.20	0.9870
14.40	1.520	63.90	1.535	4-4	120	30.70	0.7930
14.70	1.591	65.40	1.530	4-5	120	32.20	0.9910
15.80	1.514	67.90	1.526	4-6	120	33.70	0.9820
16.30	1.622	70.40	1.528	5-2	120	37.20	0.9340
16.70	1.513	70.90	1.560	5-3	120	38.70	0.9840
19.30	1.502	71.40	1.530	5-4	120	40.20	1.0730
20.00	1.530	72.40	1.540	5-5	120	41.70	0.9700
22.90	1.561	72.90	1.527	5-6	120	43.20	1.0860
23.10	1.520	73.70	1.548	6-2	120	46.70	1.0470
23.90	1.512	75.40	1.532	6-3	120	48.20	1.1650
24.10	1.540	75.70	1.563	6-4	120	49.70	1.0840
24.60	1.512	76.40	1.526	6-5	120	51.20	1.0010
24.80	1.548	76.70	1.572	6-6	120	52.70	1.1200
25.40	1.503	77.40	1.530	7-2	120	56.14	1.1960
25.90	1.515	78.40	1.528	7-3	120	57.64	1.1780
26.60	1.532	79.90	1.525	7-4	120	59.14	1.1670
27.10	1.500	81.00	1.542	7-5	120	60.64	1.1440
28.90	1.532	81.90	1.536				
29.20	1.502	82.90	1.531				
29.80	1.526	83.90	1.524				
30.90	1.523	85.00	1.533				
32.40	1.502	85.50	1.519				
33.10	1.535	86.50	1.536				
34.20	1.501	87.60	1.550				
35.40	1.528	88.40	1.528				
36.40	1.507	89.90	1.522				
38.10	1.529	90.40	1.525				
39.40	1.510	91.40	1.528				
41.40	1.580	92.40	1.525				
42.10	1.540	93.40	1.526				
42.90	1.525	94.40	1.520				
44.90	1.525	95.40	1.520				
46.40	1.535	96.40	1.520				
47.40	1.515	97.40	1.535				
47.70	1.548	97.90	1.522				

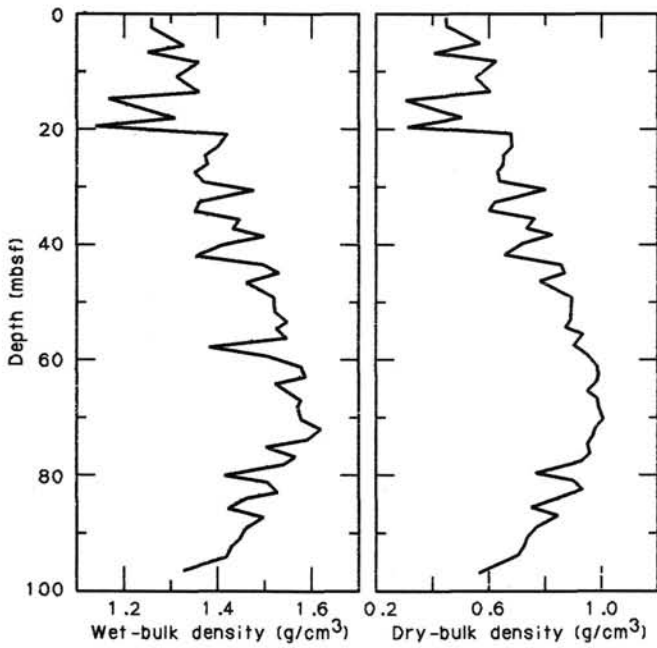


Figure 16. Wet- and dry-bulk-density profiles for Hole 665A.

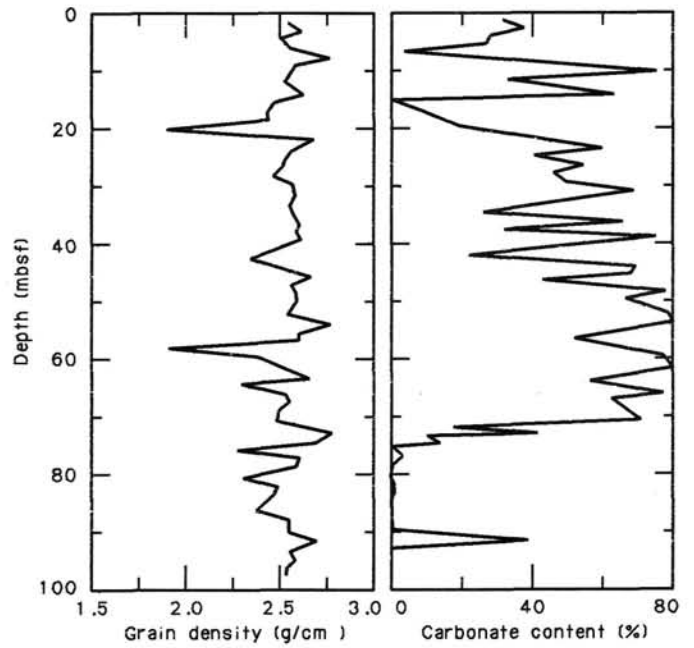


Figure 18. Grain-density and calcium carbonate profiles for Hole 665A.

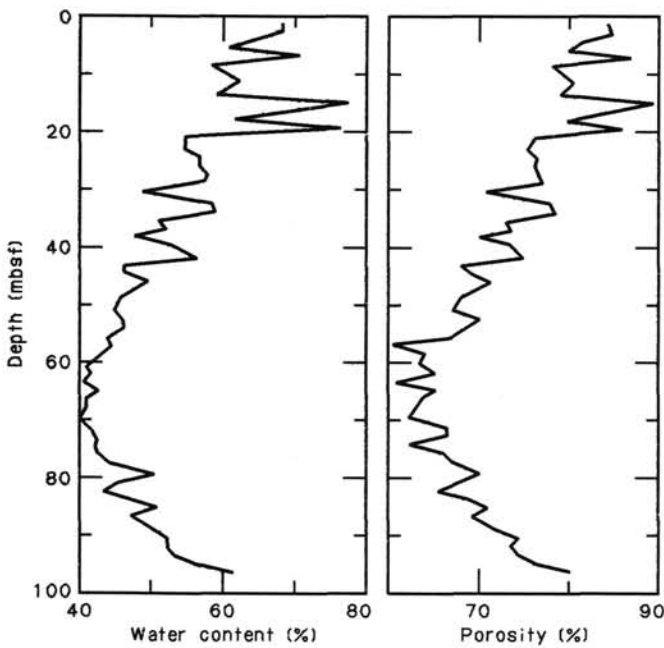


Figure 17. Water-content and porosity profiles for Hole 665A.

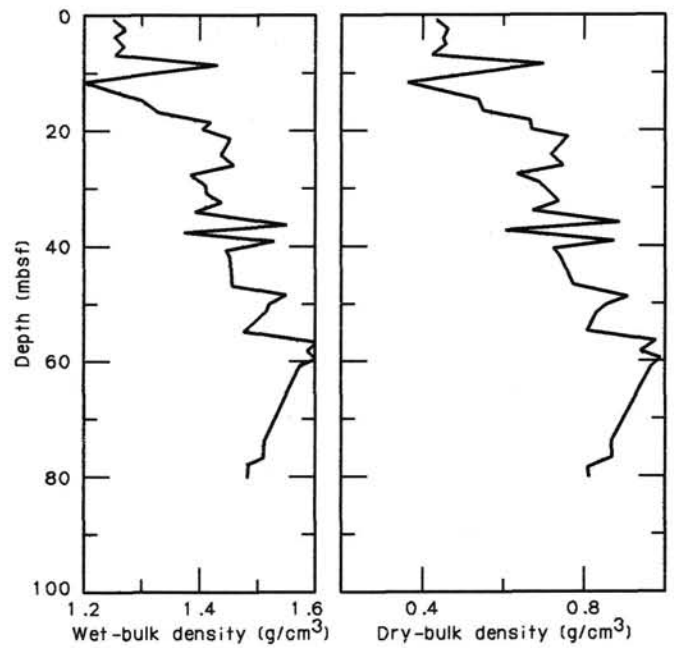


Figure 19. Wet- and dry-bulk-density profiles for Hole 665B.

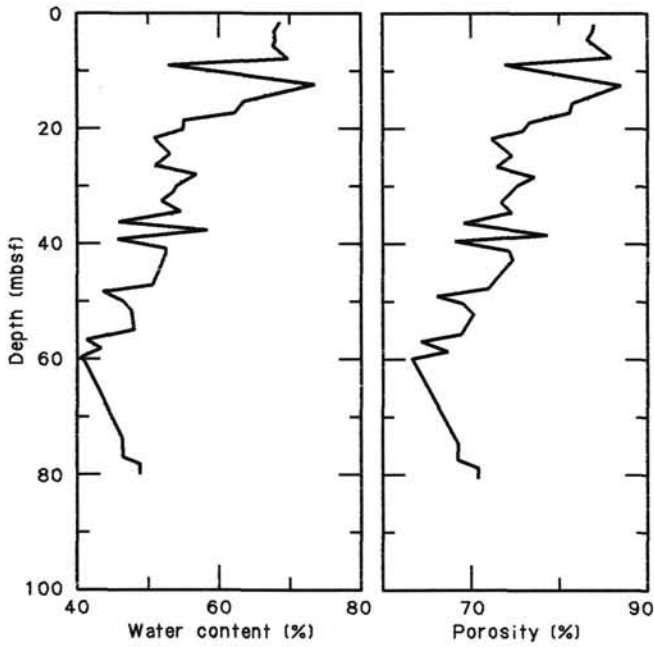


Figure 20. Water-content and porosity profiles for Hole 665B.

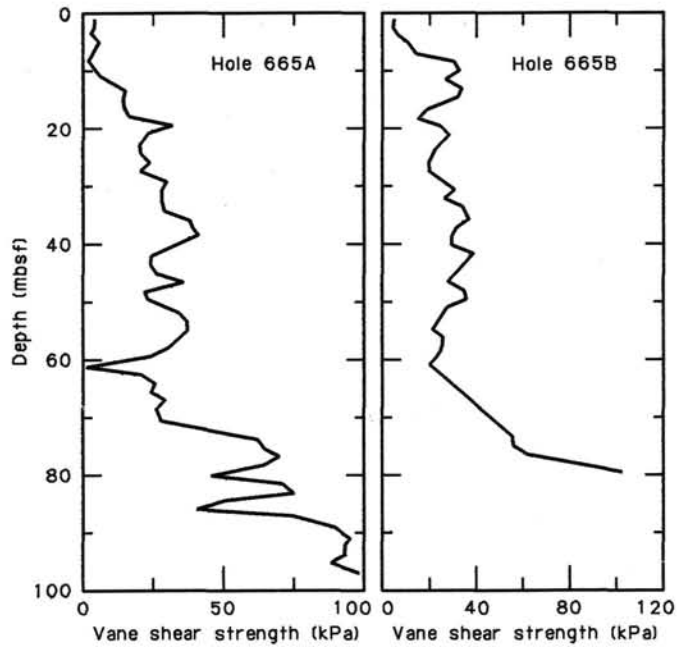


Figure 21. Vane-shear-strength profiles for Site 665.

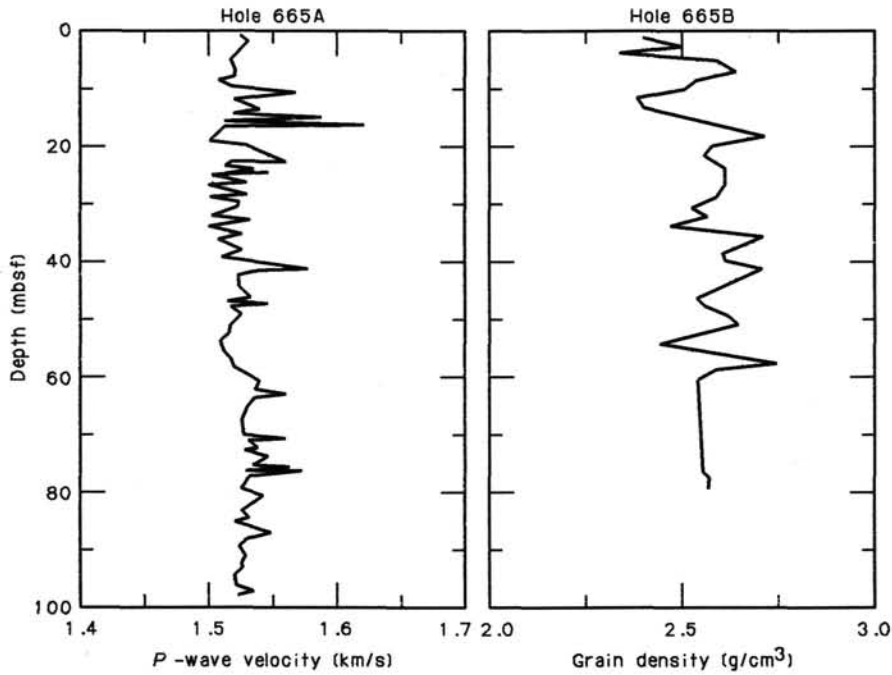


Figure 22. *P*-wave-velocity profile for Hole 665A and grain density profile from Hole 665B.

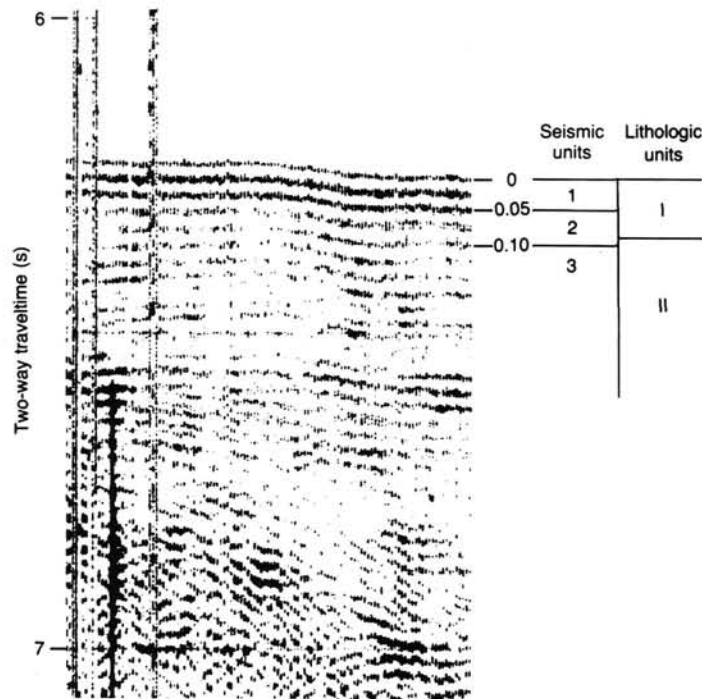


Figure 23. Comparison of Site 665 seismic units with lithologic units. All depths in seconds of two-way travellime.

Table 10. Composite-depth sections between Holes 665A and 665B.

Hole 665A Interval (cm)	Hole 665B Interval (cm)	Composite depths (mbsf)
1H-1, 0		0
↓		
1H-2, 106> 1H-2, 112	2.56
↓	↓	
2H-2, 7	<..... 1H-4, 64	4.98
↓	↓	
2H-6, 115> 2H-3, 82	11.76
↓	↓	
3H-1, 70	<..... 2H-5, 22	14.16
↓	↓	
3H-6, 100> 3H-3, 16	21.96
↓	↓	
4H-1, 121	<..... 3H-5, 49	25.26
↓	↓	
4H-7, 19> 4H-3, 31	33.24
↓	↓	
5H-1, 34	<..... 4H-4, 133	35.76
↓	↓	
5H-7, 14> 5H-4, 34	45.24
↓	↓	
6H-3, 50	<..... 5H-6, 70	48.60
↓	↓	
6H-7, 40> 6H-5, 0	54.40
↓	↓	
7H-1, 55	<..... 6H-6, 44	56.34
↓	↓	
7H-7, 20> 7H-4, 43	64.89
↓	↓	
8H-1, 82	<..... 7H-5, 7	66.03
↓	↓	
8H-2, 55> 7H-6, 7	67.26

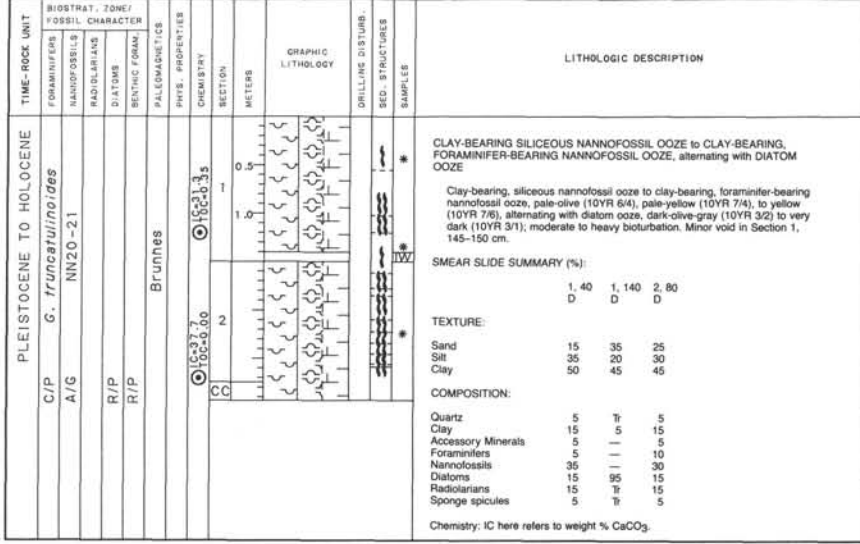
Note: Correlative levels in each core are shown alongside the composite depths calculated by adding together (from the top of the hole) the lengths of individual sections. Arrows indicate the pathway of the correlation sequence. Hole 665A is used as the major pathway.

Table 11. Composite-depth sections between Holes 665B and 665A.

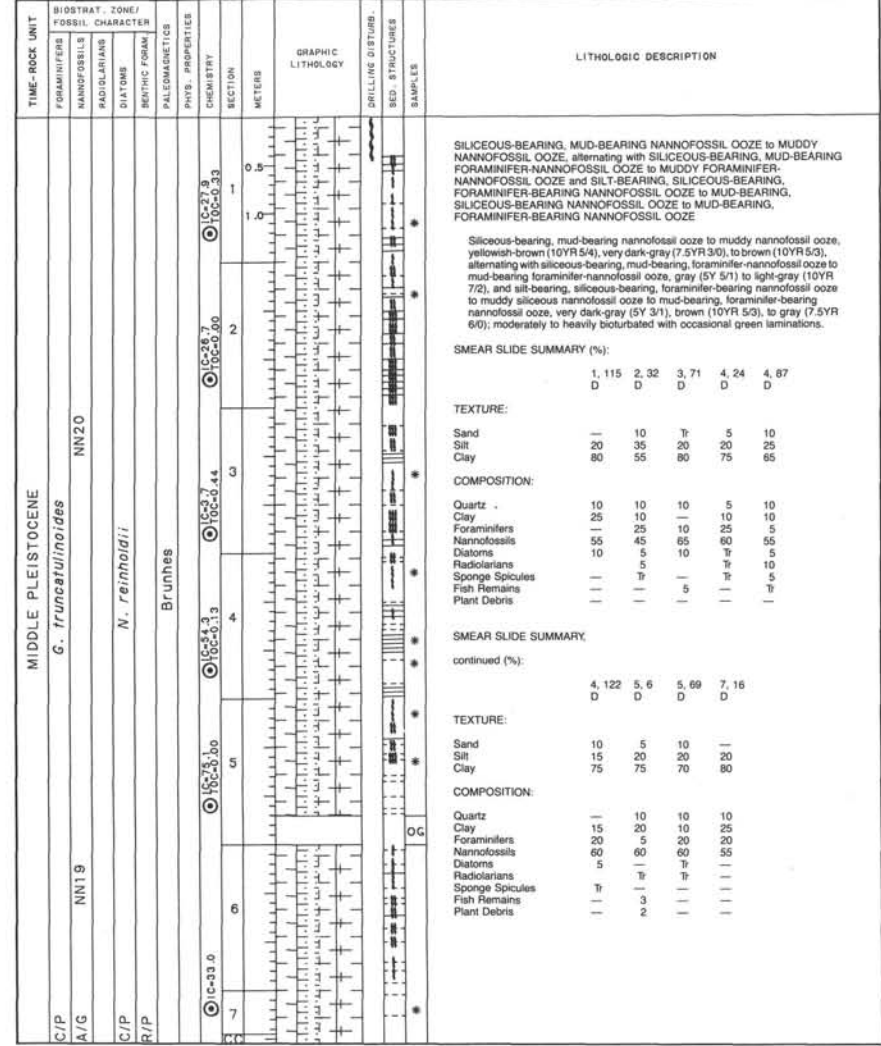
Hole 665B Interval (cm)	Hole 665A Interval (cm)	Composite depths (mbsf)
1H-1, 0		0
↓		
1H-4, 112> 2H-2, 55	5.62
↓	↓	
2H-1, 25	<..... 2H-4, 37	8.44
↓	↓	
2H-7, 16> 3H-3, 88	17.35
↓	↓	
3H-1, 58	<..... 3H-5, 7	19.54
↓	↓	
3H-6, 106> 4H-3, 37	27.52
↓	↓	
4H-1, 106	<..... 4H-5, 85	31.00
↓	↓	
4H-7, 7> 5H-3, 26	39.01
↓	↓	
5H-1, 82	<..... 5H-4, 64	40.89
↓	↓	
5H-6, 70> 6H-3, 50	48.77
↓	↓	
6H-2, 46	<..... 6H-4, 49	50.26
↓	↓	
6H-6, 44> 7H-1, 55	56.24
↓	↓	
7H-1, 34	<..... 7H-3, 148	60.17
↓	↓	
7H-6, 7> 8H-2, 55	67.40

Note: Correlative levels in each core are shown adjacent to the composite depths calculated by adding together (from the top of the hole) the lengths of individual sections. Arrows indicate the pathway of the correlation sequence. Hole 665B is used as the major pathway.

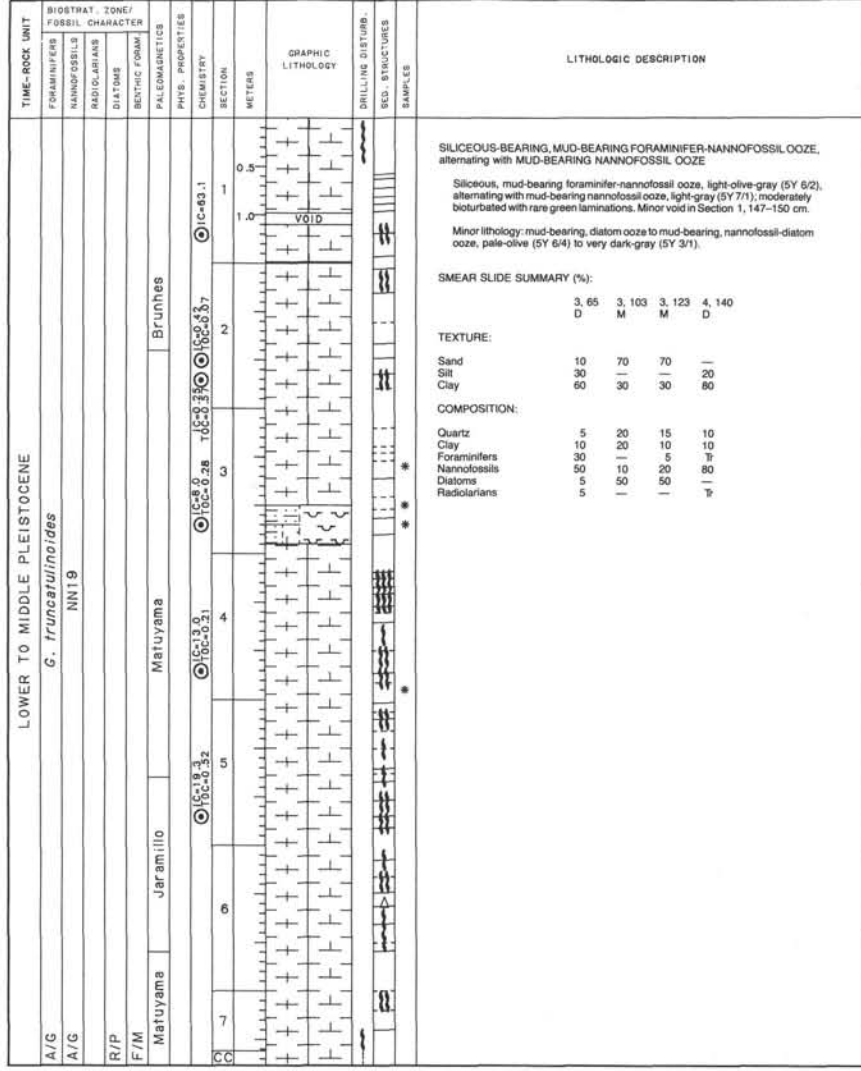
SITE 665 HOLE A CORE 1 H CORED INTERVAL 4740.4-4743.3 mbsi; 0-2.9 mbsf



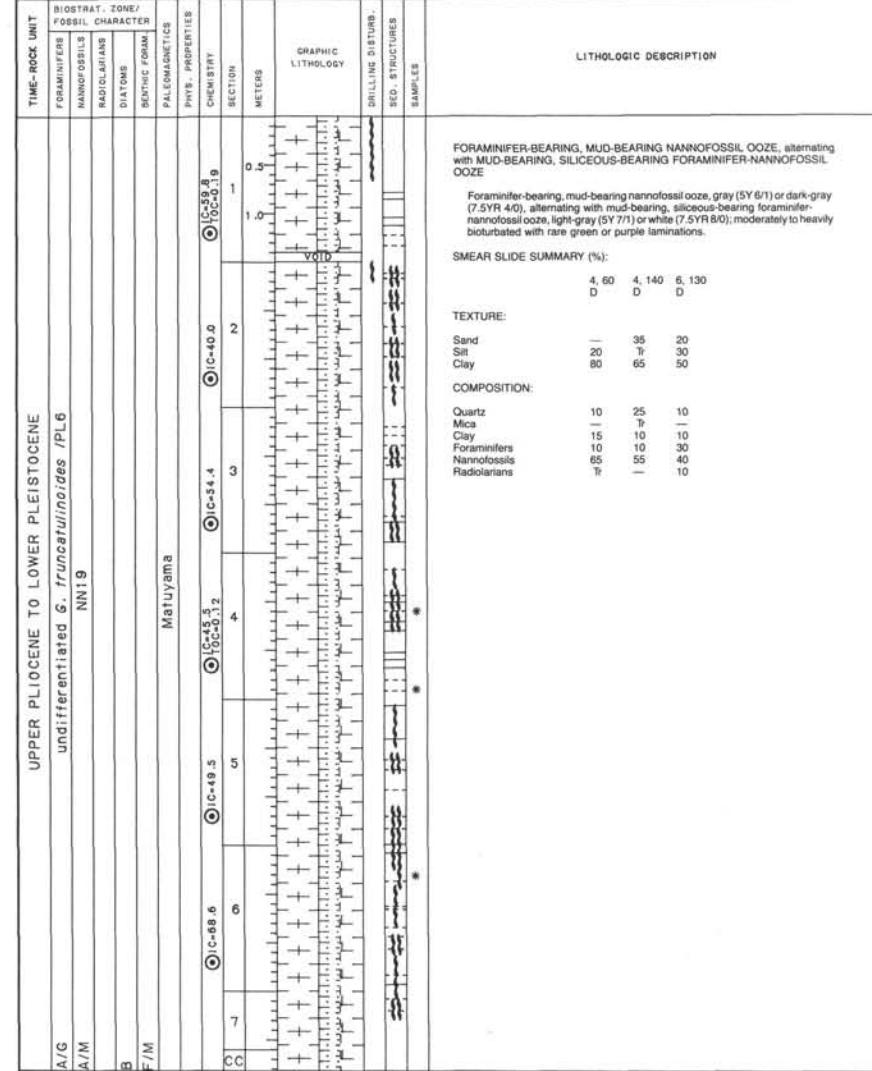
SITE 665 HOLE A CORE 2 H CORED INTERVAL 4743.3-4752.8 mbsi; 2.9-12.4 mbsf



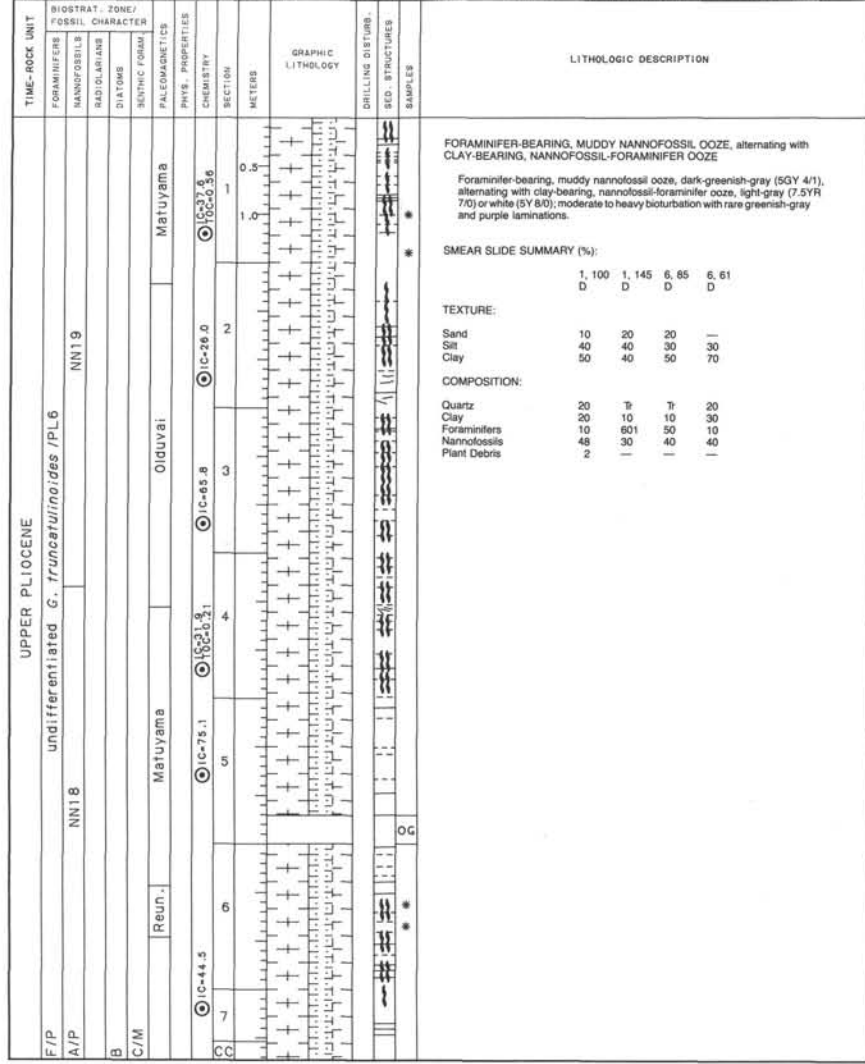
SITE 665 HOLE A CORE 3 H CORED INTERVAL 4752.8-4762.3 mbsl; 12.4-21.9 mbsf



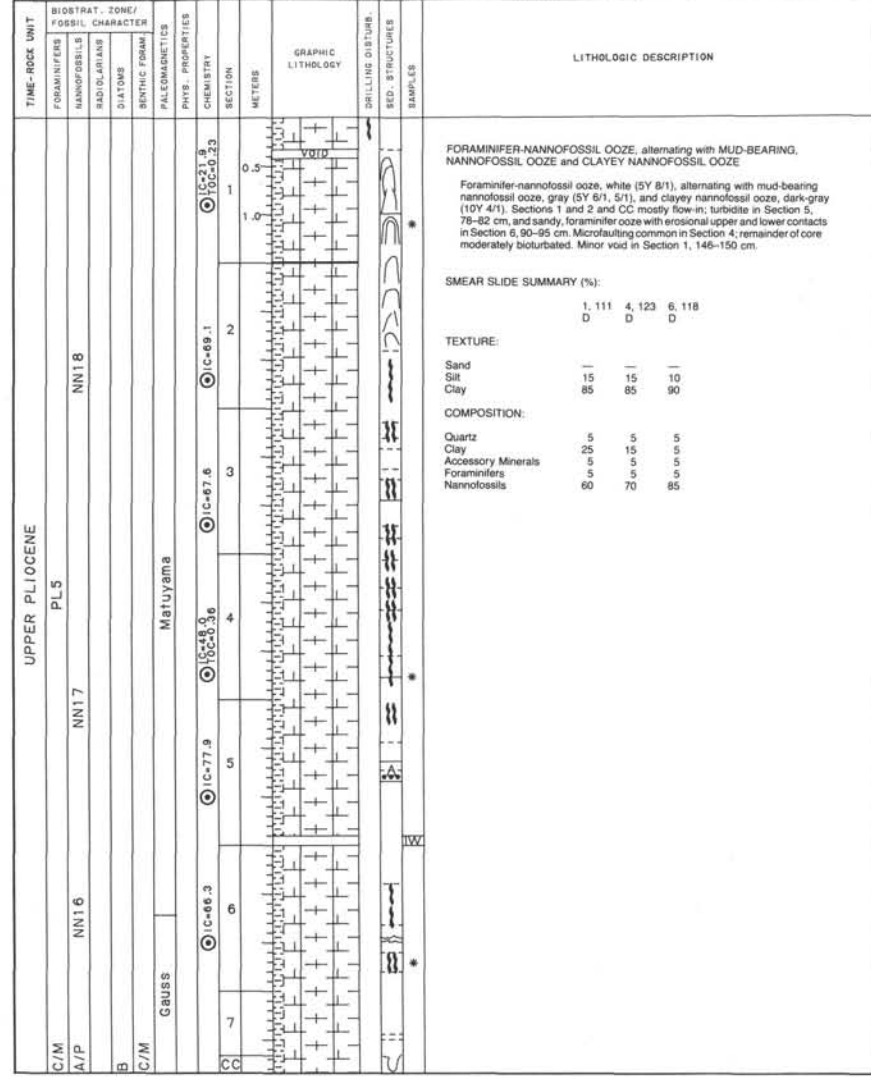
SITE 665 HOLE A CORE 4 H CORED INTERVAL 4762.3-4771.8 mbsl; 21.9-31.4 mbsf



SITE 665 HOLE A CORE 5 H CORED INTERVAL 4771.8-4281.3 mbsf; 31.4-40.9 mbsf



SITE 665 HOLE A CORE 6 H CORED INTERVAL 4781.3-4790.8 mbsf; 40.9-50.4 mbsf



SITE 665 HOLE A CORE 7 H CORED INTERVAL 4790.8-4800.3 mbsl; 50.4-59.9 mbsf

TIME-ROCK UNIT		BIOSTRAT. ZONE/ FOSSIL CHARACTER	SECTION	METERS	GRAPHIC LITHOLOGY	DRILLING DISTURB.	SED. STRUCTURES	SAMPLES	LITHOLOGIC DESCRIPTION
FORAMINIFERS	NANNOFOSSILS								
UPPER PLIOCENE									
A/M	PL3								
A/M	PL4 A/M								
	NN16								
B									
F/M									
GAUSS									
			1	0.5					
			1	1.0					
			2						
			3						
			4						
			5						
			6						
			7						
			8						
			9						
			10						
			11						
			12						
			13						
			14						
			15						
			16						
			17						
			18						
			19						
			20						
			21						
			22						
			23						
			24						
			25						
			26						
			27						
			28						
			29						
			30						
			31						
			32						
			33						
			34						
			35						
			36						
			37						
			38						
			39						
			40						
			41						
			42						
			43						
			44						
			45						
			46						
			47						
			48						
			49						
			50						
			51						
			52						
			53						
			54						
			55						
			56						
			57						
			58						
			59						
			60						
			61						
			62						
			63						
			64						
			65						
			66						
			67						
			68						
			69						
			70						
			71						
			72						
			73						
			74						
			75						
			76						
			77						
			78						
			79						
			80						
			81						
			82						
			83						
			84						
			85						
			86						
			87						
			88						
			89						
			90						
			91						
			92						
			93						
			94						
			95						
			96						
			97						
			98						
			99						
			100						

FORAMINIFER-NANNOFOSSIL OOZE, alternating with MUDDY NANNOFOSSIL OOZE

Foraminifer-nannofossil ooze, white (7.5YR 8/0 and 10Y 8/1), alternating with muddy nannofossil ooze, light-gray (10Y 7/1, 7.5YR 7/0) or light-brownish-gray (2.5Y 6/2); weak to moderate bioturbation; turbidite in Section 5, 100 cm.

SMEAR SLIDE SUMMARY (%):

	5, 80	7, 20
D	D	D

TEXTURE:

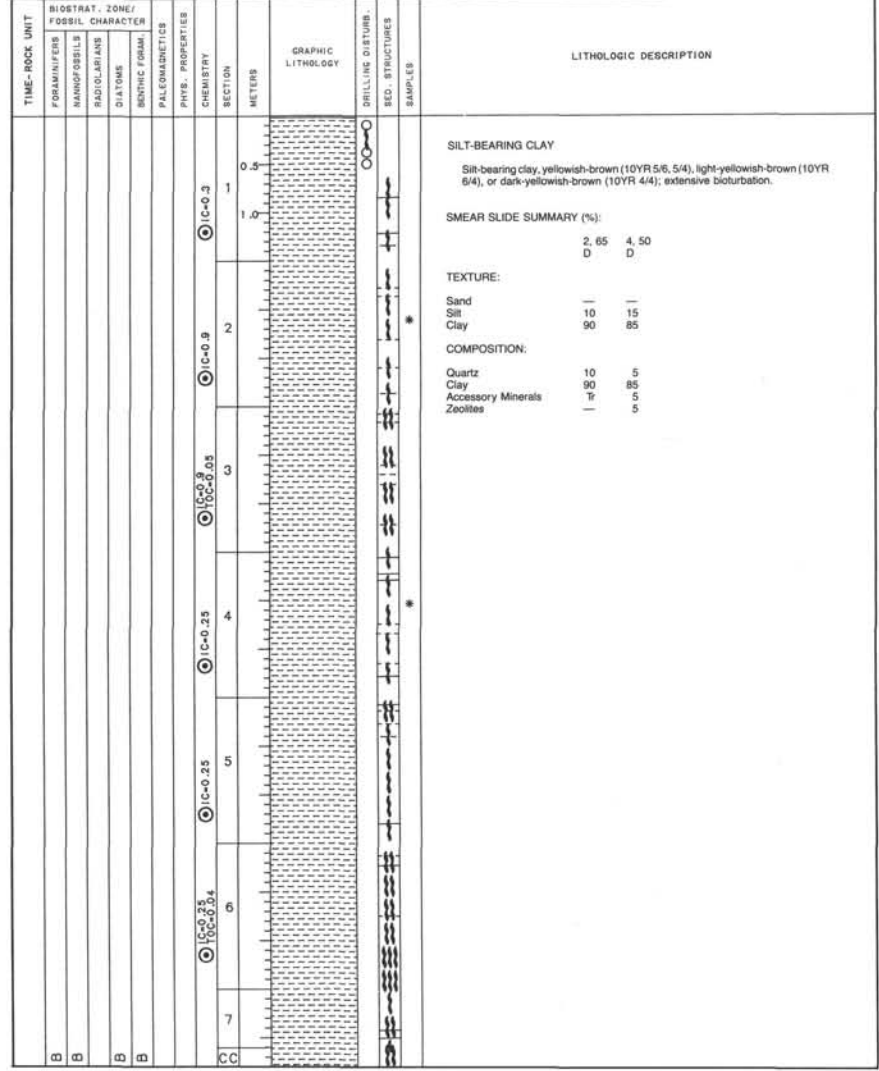
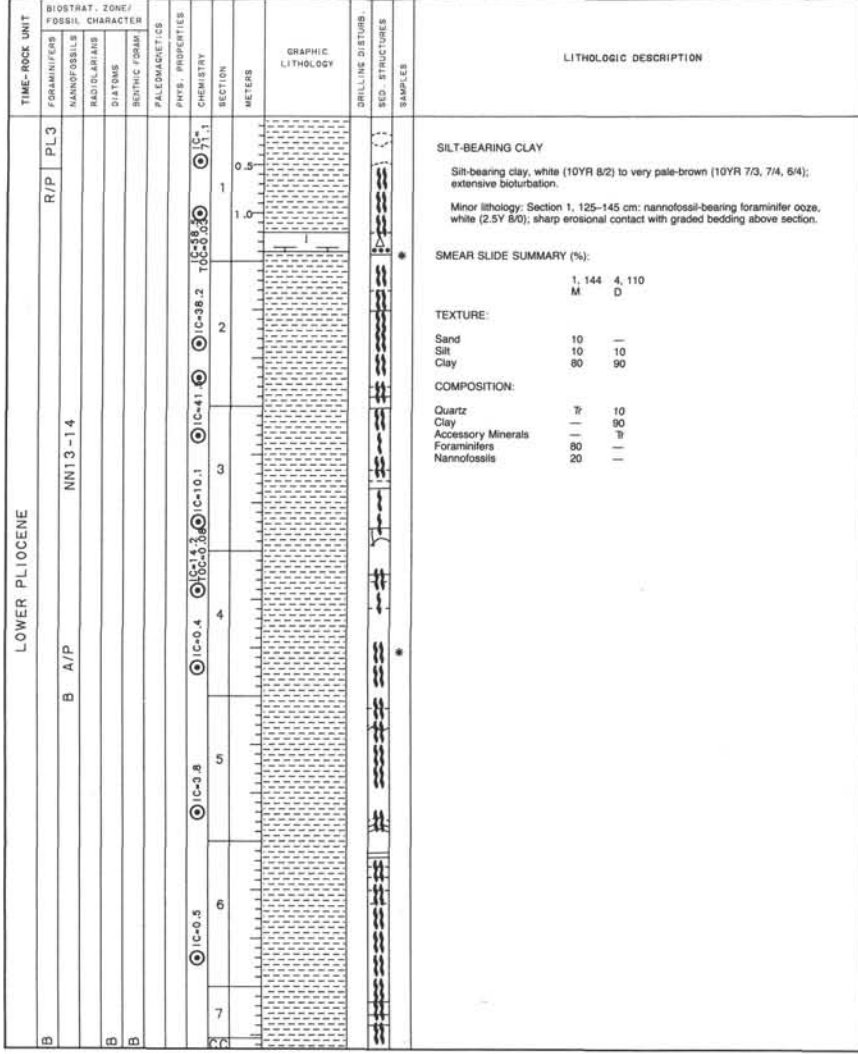
Sand	—	25
Silt	30	10
Clay	70	65

COMPOSITION:

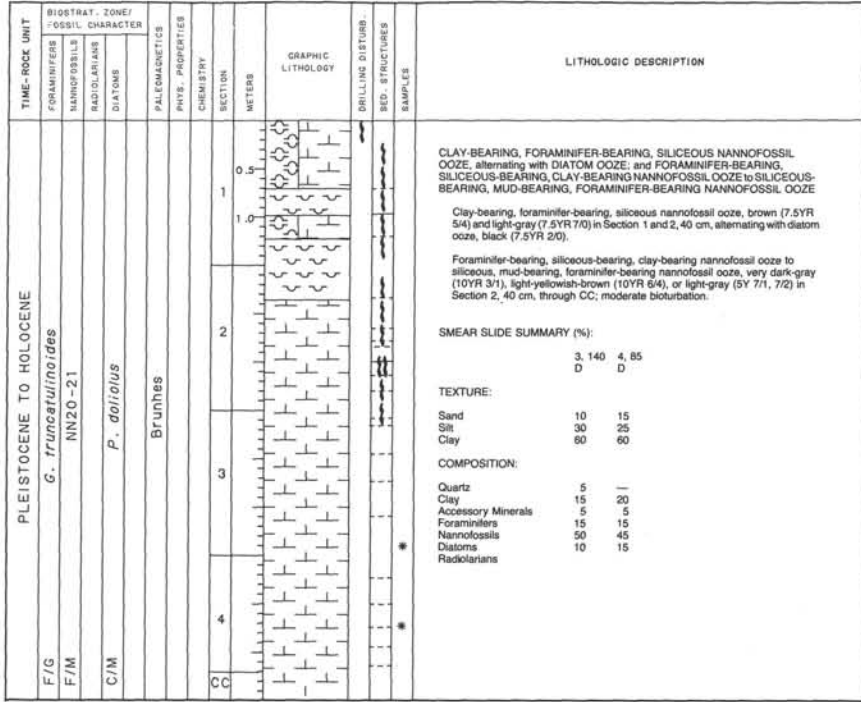
Quartz	5	5
Clay	5	—
Accessory Minerals	20	Tr
Foraminifers	5	30
Nannofossils	65	65

SITE 665 HOLE A CORE 8 H CORED INTERVAL 4800.3-4809.8 mbsl; 59.9-69.4 mbsf

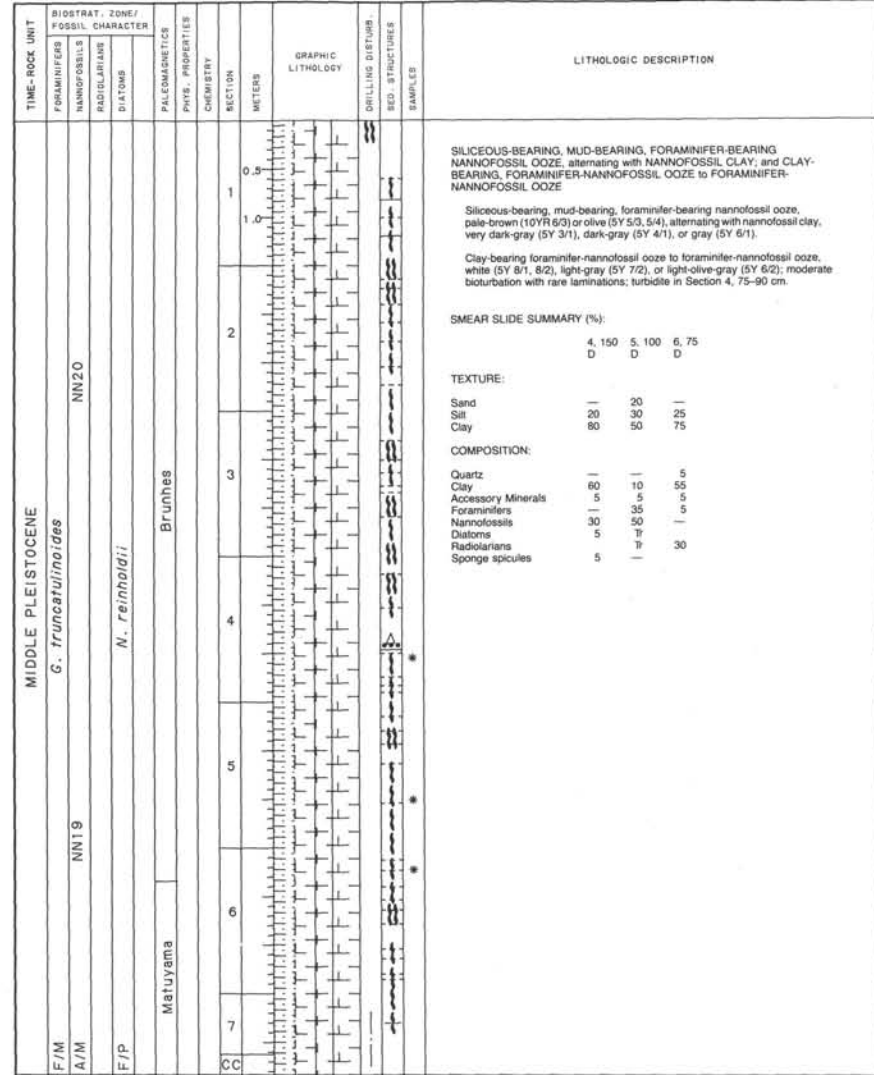
TIME-ROCK UNIT		BIOSTRAT. ZONE/ FOSSIL CHARACTER	SECTION	METERS	GRAPHIC LITHOLOGY	DRILLING DISTURB.	SED. STRUCTURES	SAMPLES	LITHOLOGIC DESCRIPTION
FORAMINIFERS	NANNOFOSSILS								
UPPER PLIOCENE									
CP									
A/D	PL3								
B	NN15								
R/P									
GAUSS									
			1	0.5					
			1	1.0					
			2						
			3						
			4						
			5						
			6						
			7						
			8						
			9						
			10						
			11						
			12						
			13						
			14						
			15						
			16						
			17						
			18						
			19						
			20						
			21						
			22						
			23						
			24						
			25						
			26						
			27						
			28						
			29						
			30						
			31						
			32						
			33						
			34						
			35						
			36						
			37						
			38						
			39						
			40						
			41						
			42						
			43						
			44						
			45						
			46						
			47						
			48						
			49						
			50						
			51						
			52						
			53						
			54						
			55						
			56						
			57						
			58						
			59						
			60						
			61						
			62						
			63						
			64						
			65						
			66						
			67						
			68						
			69						

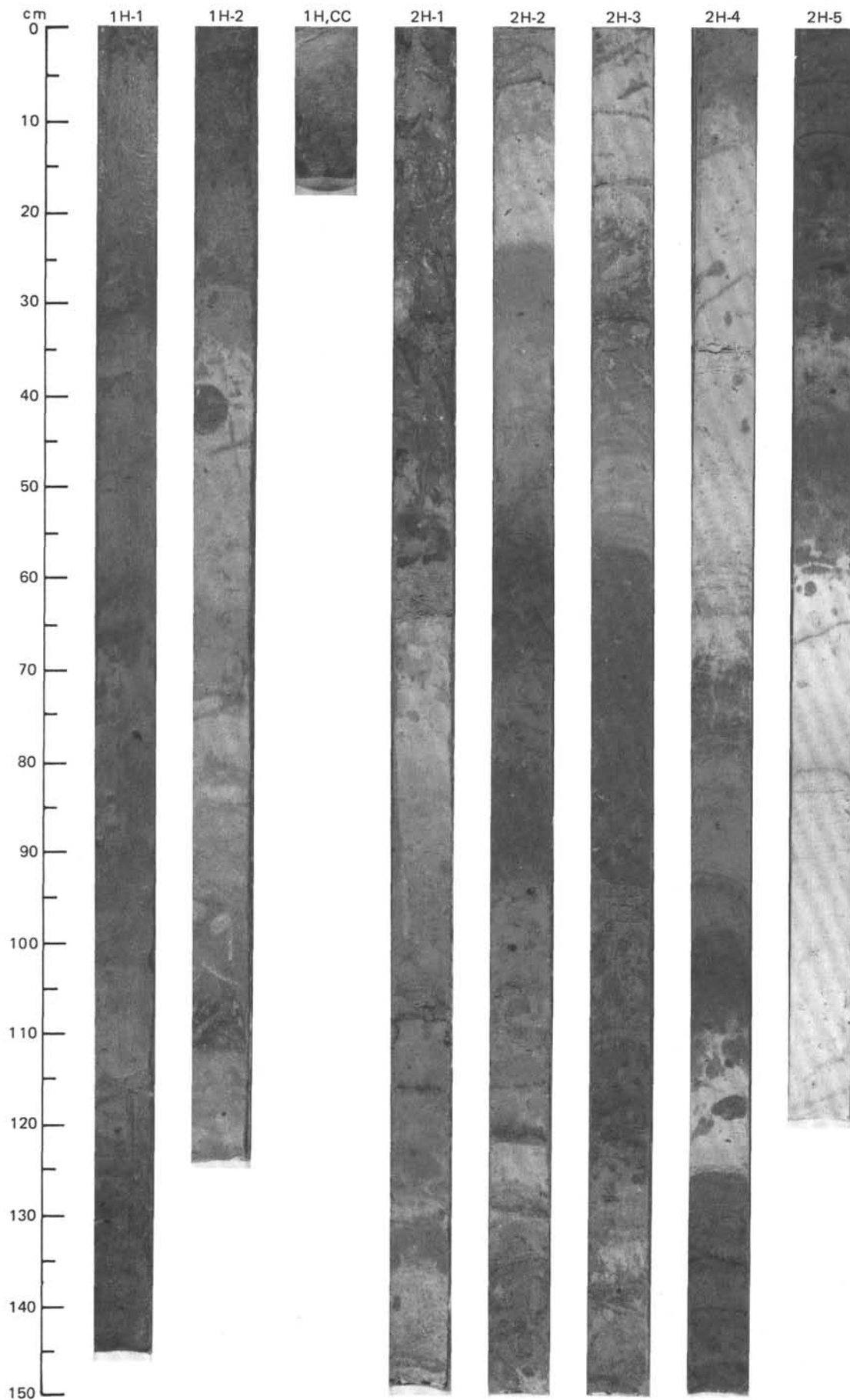


SITE 665 HOLE B CORE 1 H CORED INTERVAL 4741.8-4747.8 mbsl; 0-6.0 mbsf

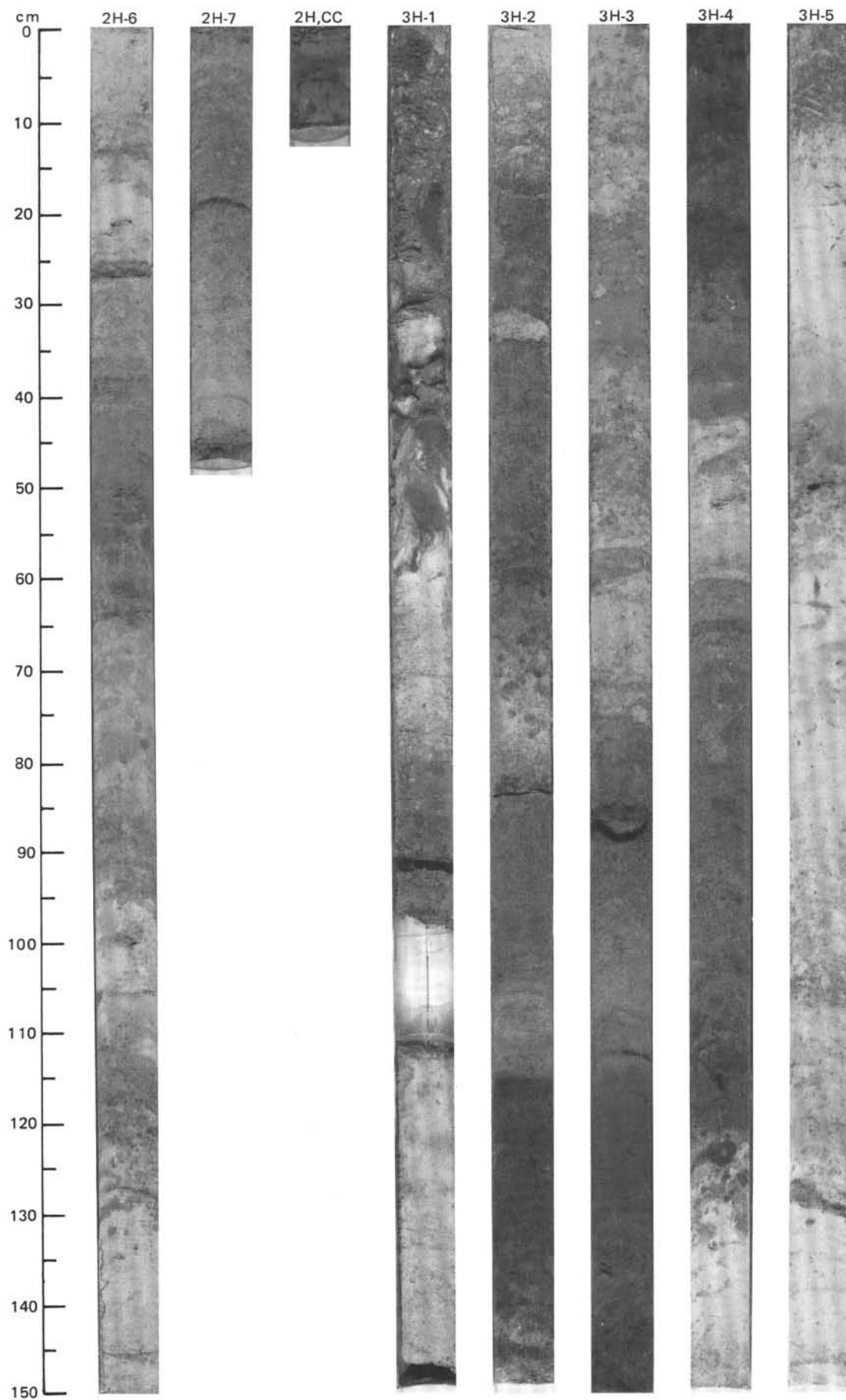


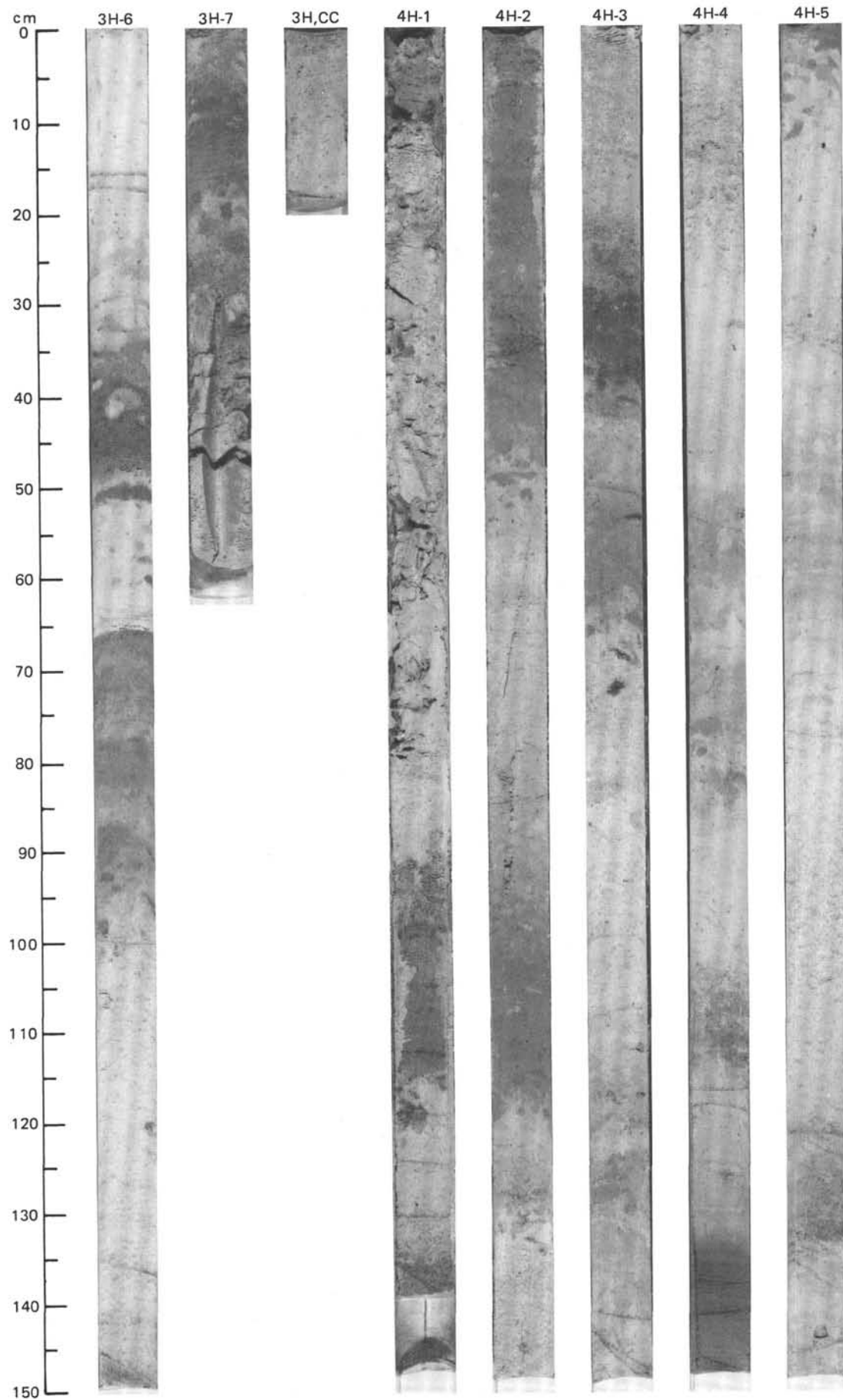
SITE 665 HOLE B CORE 2 H CORED INTERVAL 4747.8-4757.3 mbsl; 6.0-15.5 mbsf



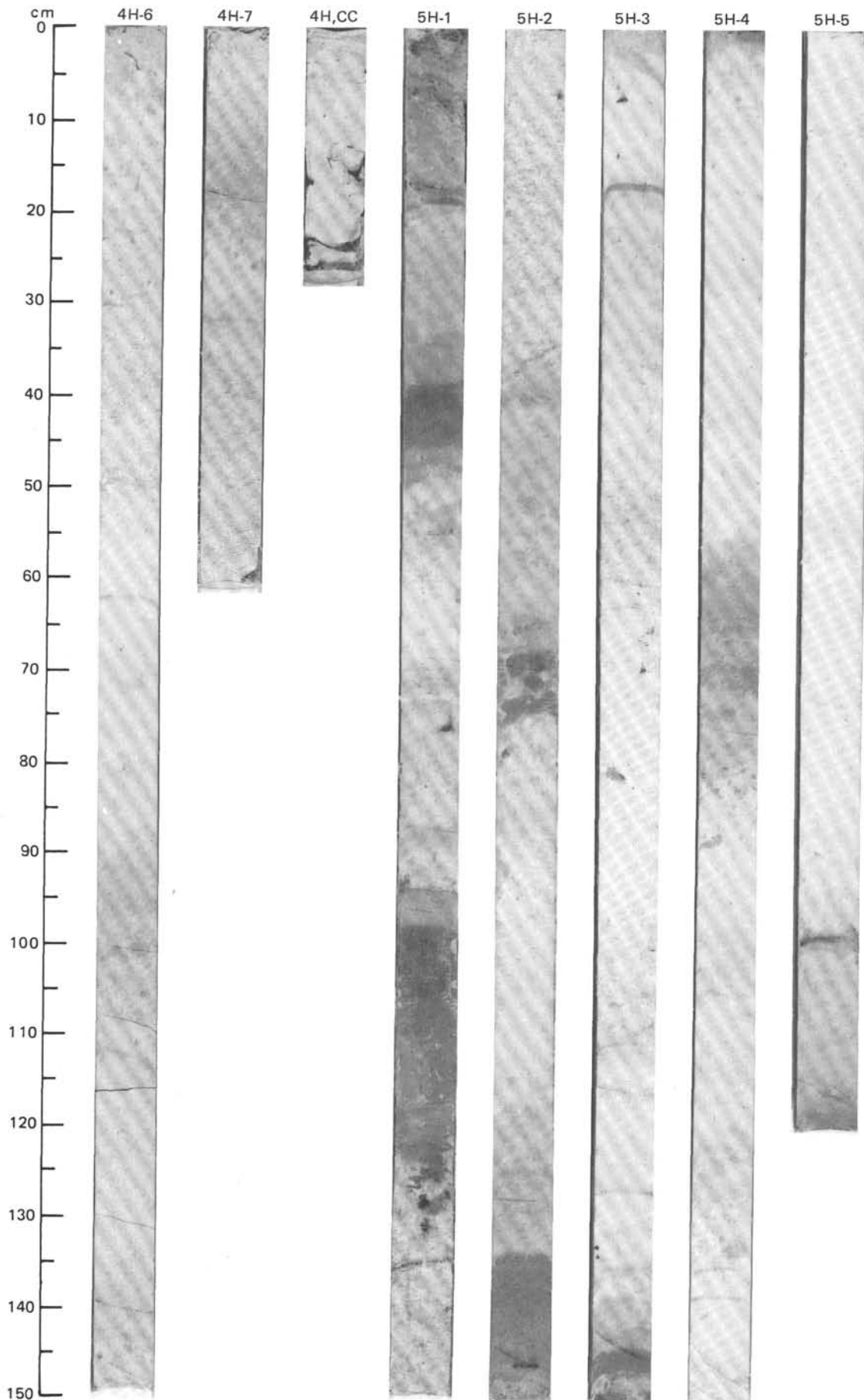


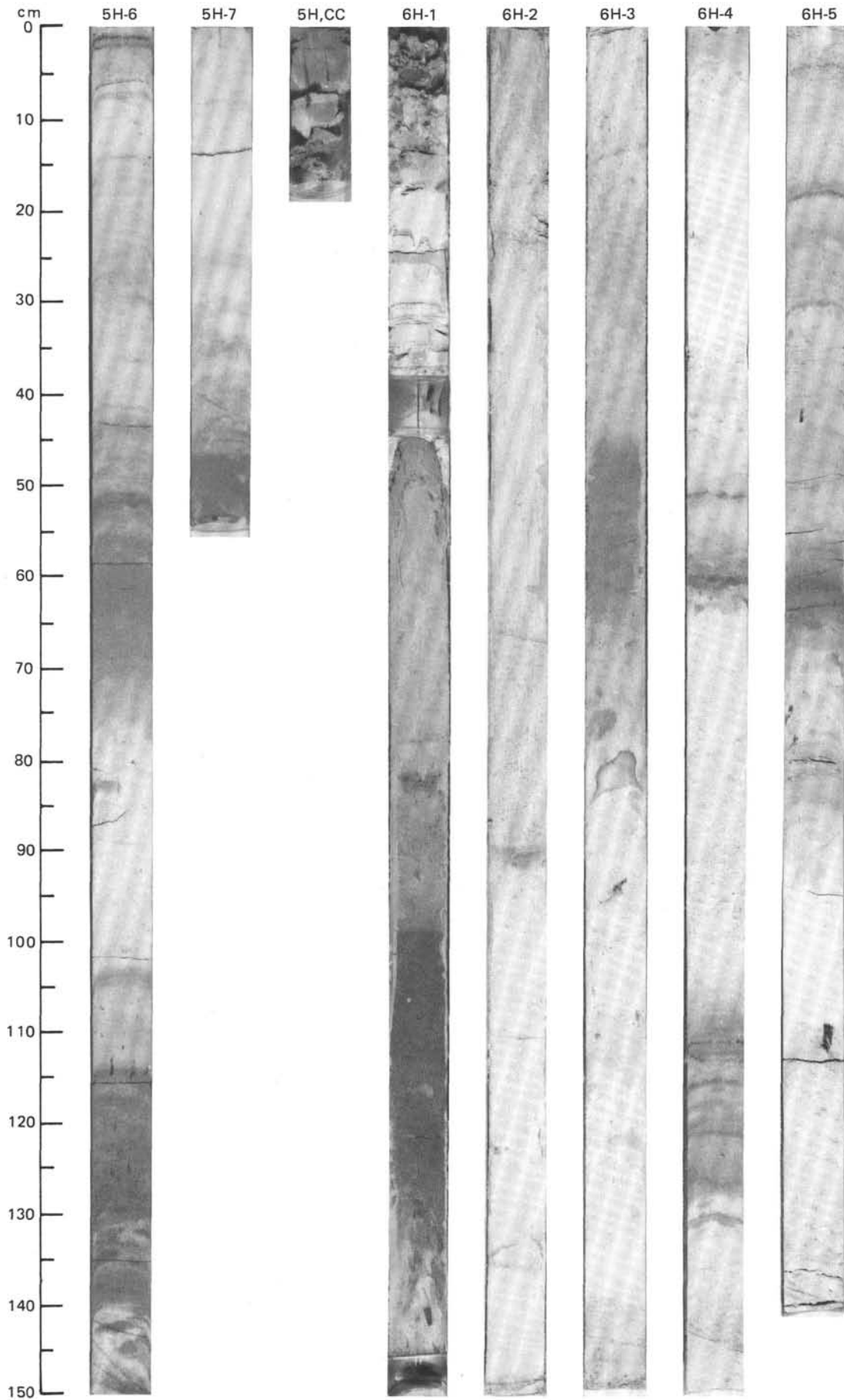
SITE 665 (HOLE A)



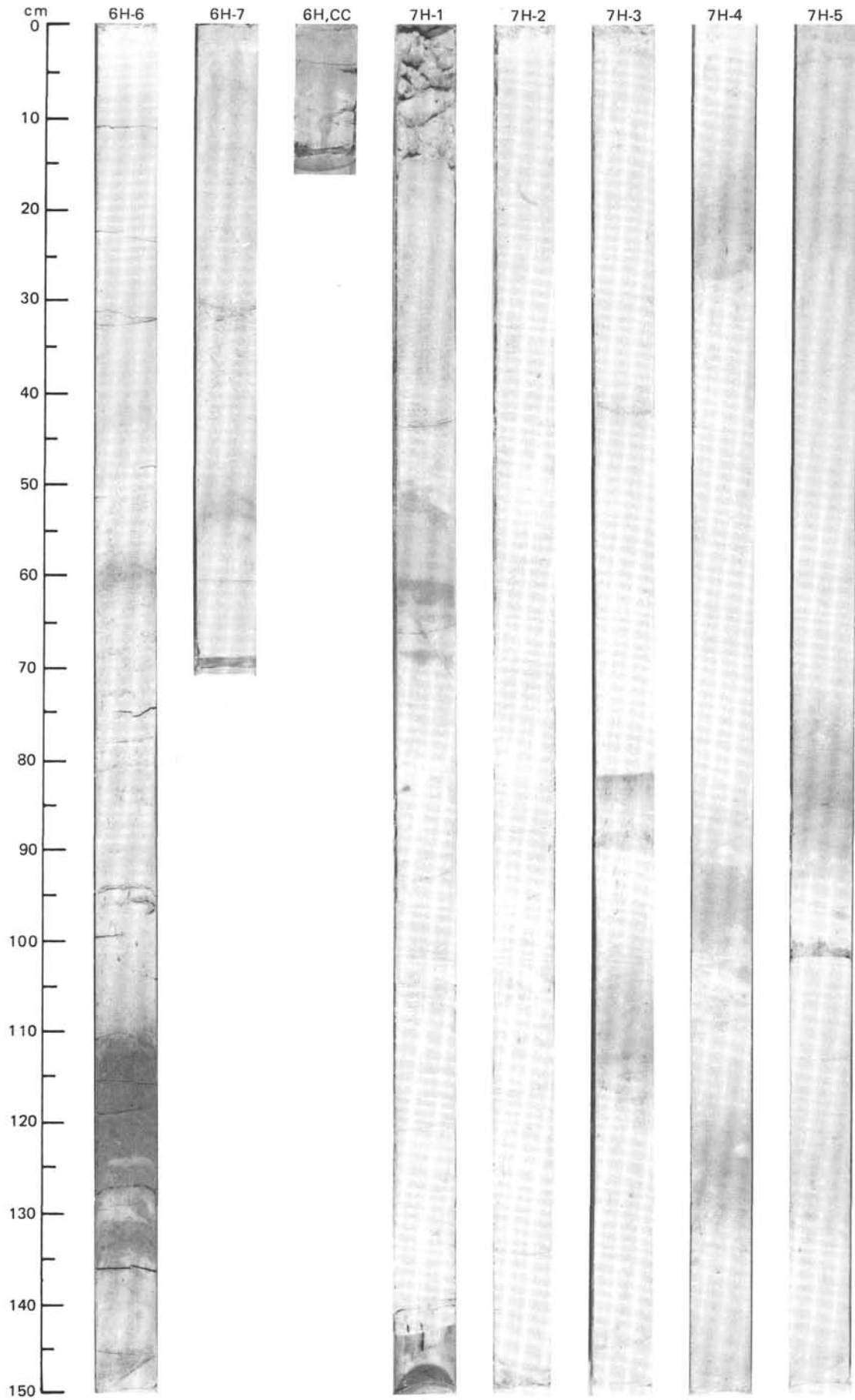


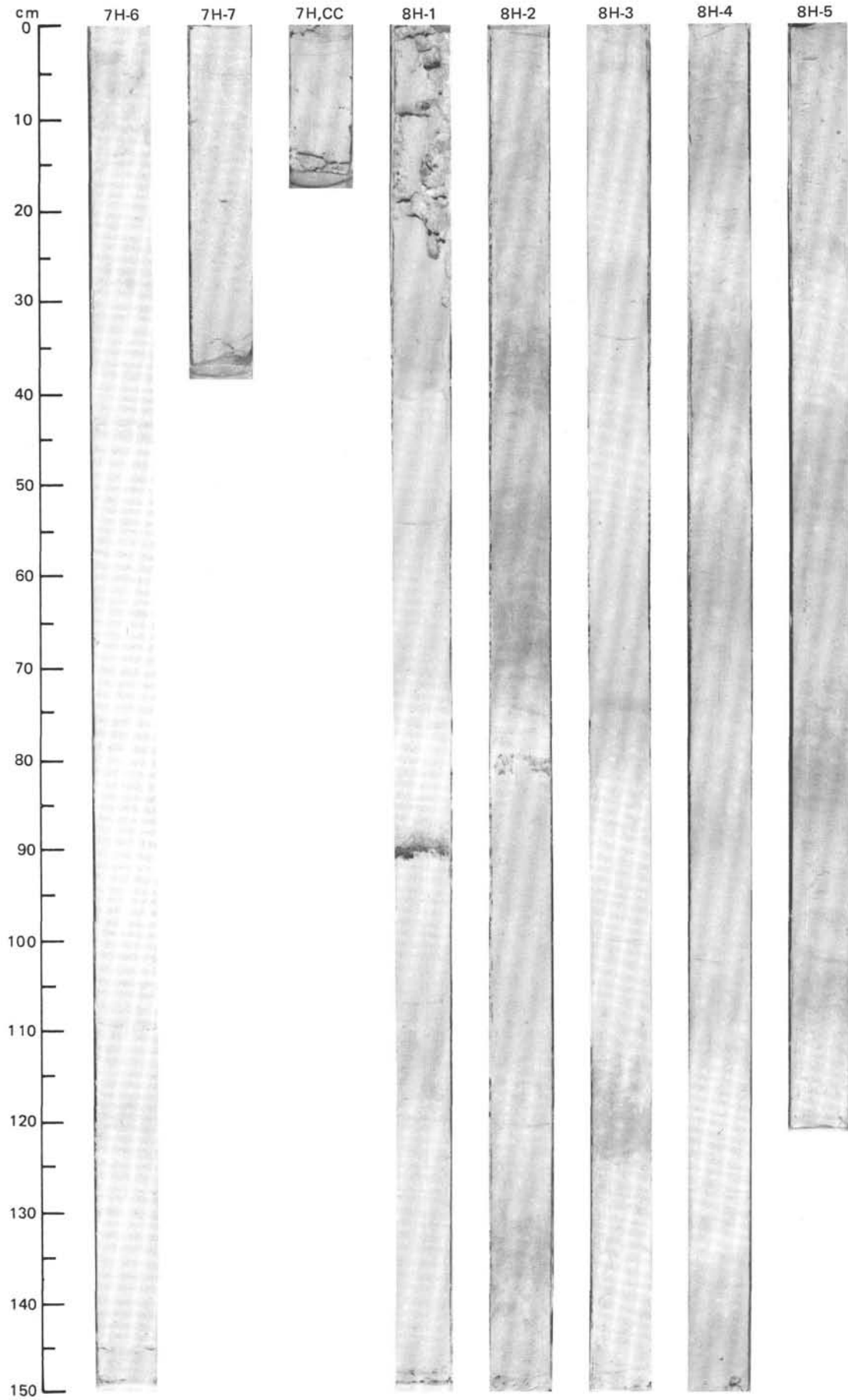
SITE 665 (HOLE A)



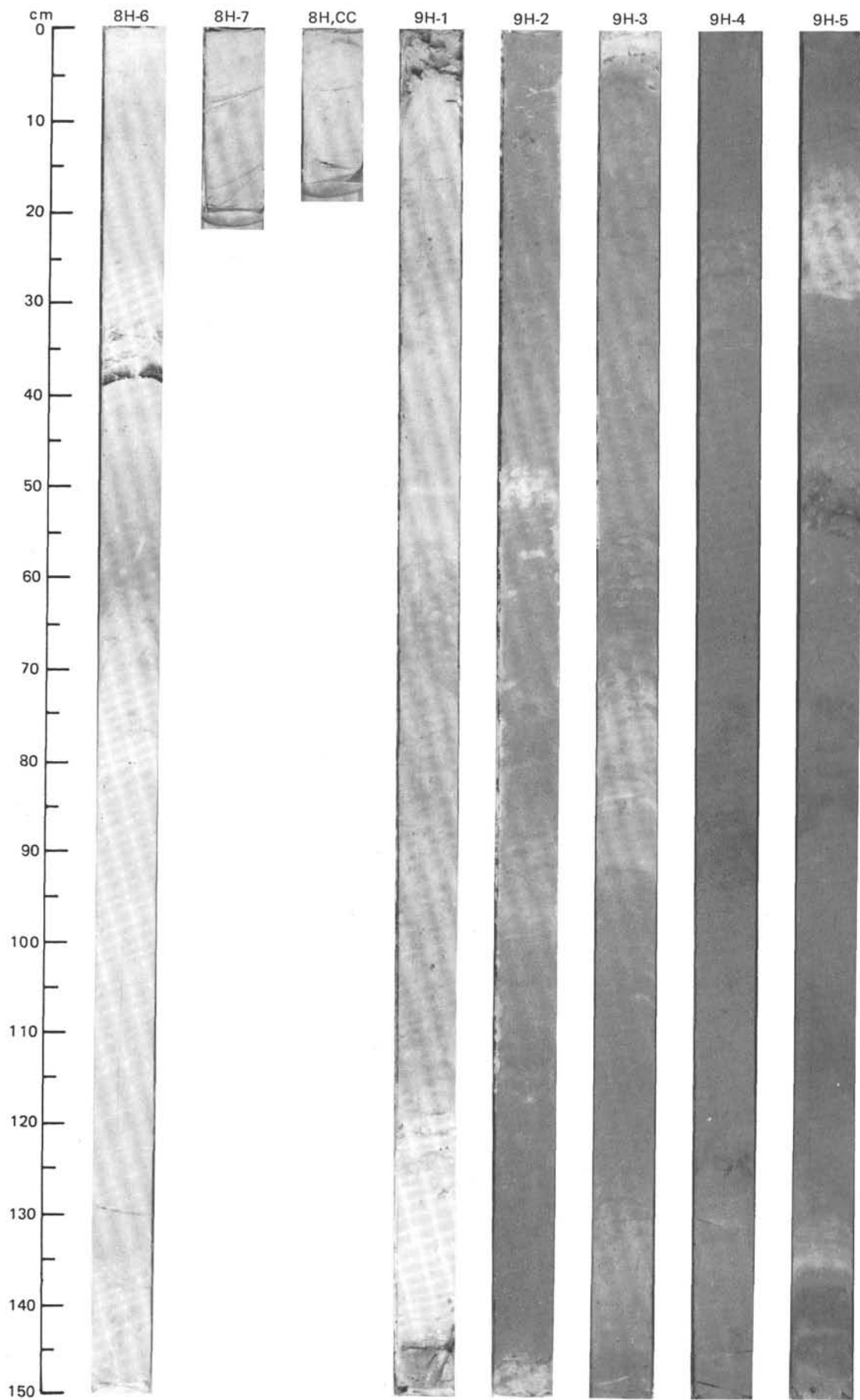


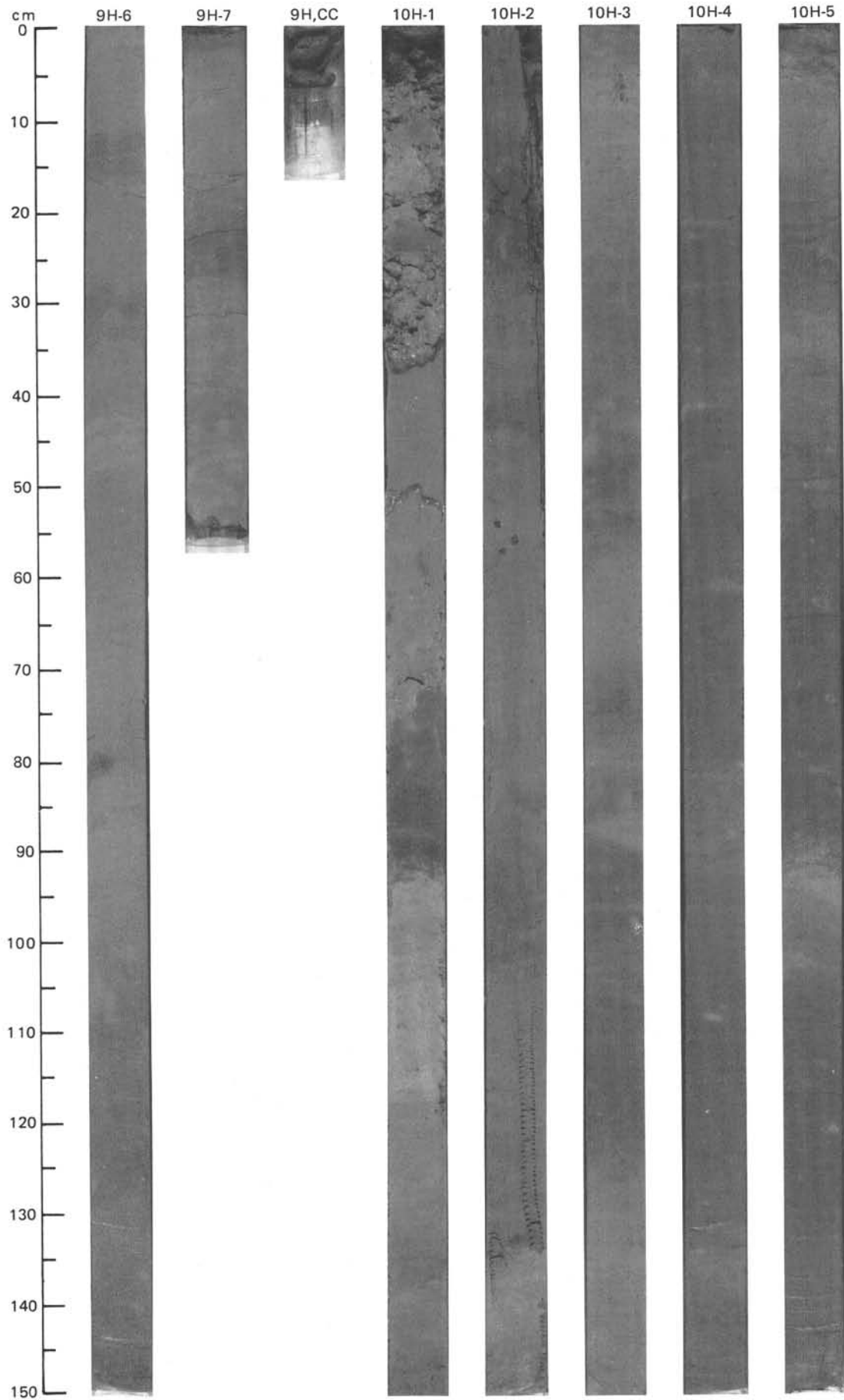
SITE 665 (HOLE A)



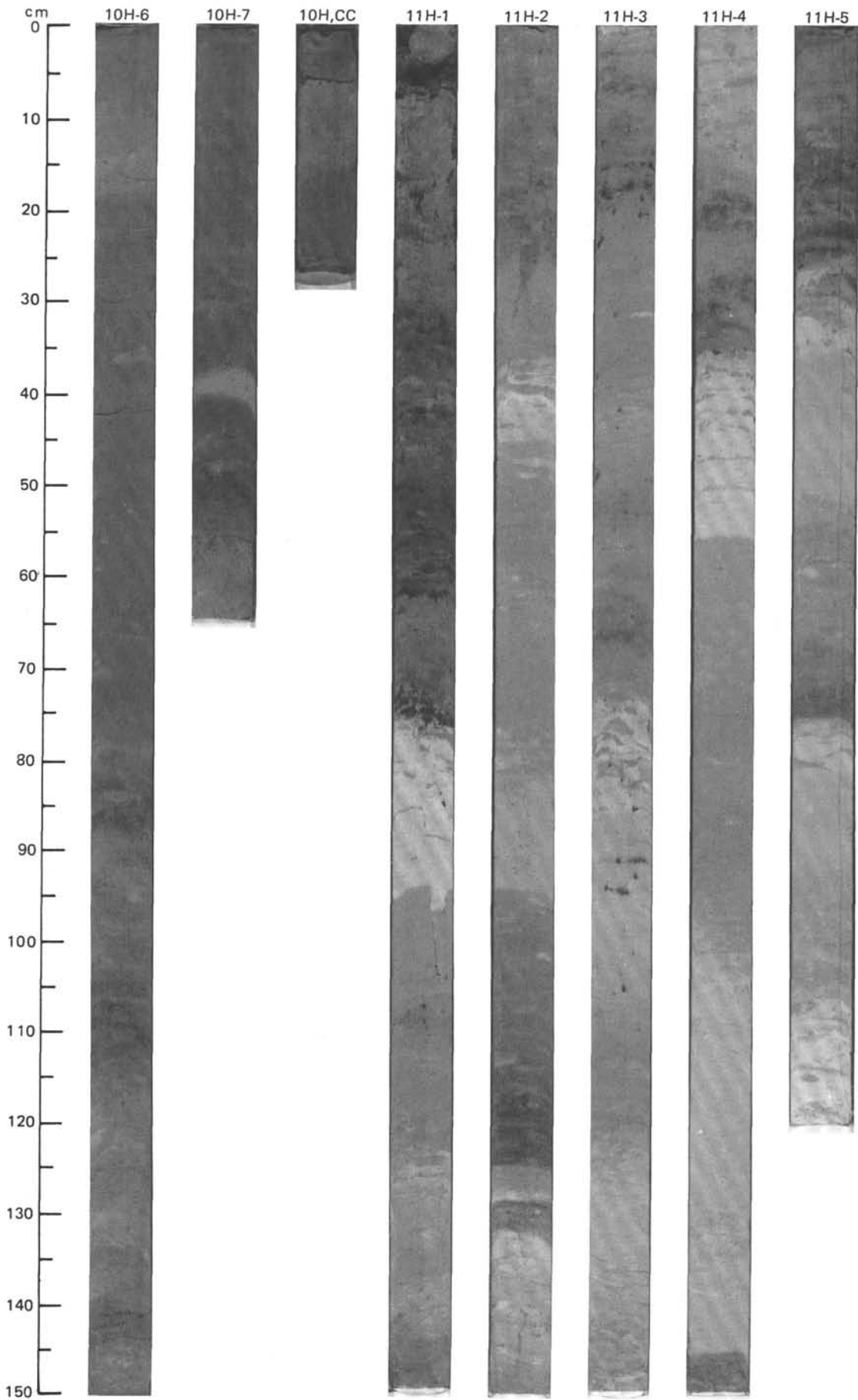


SITE 665 (HOLE A)





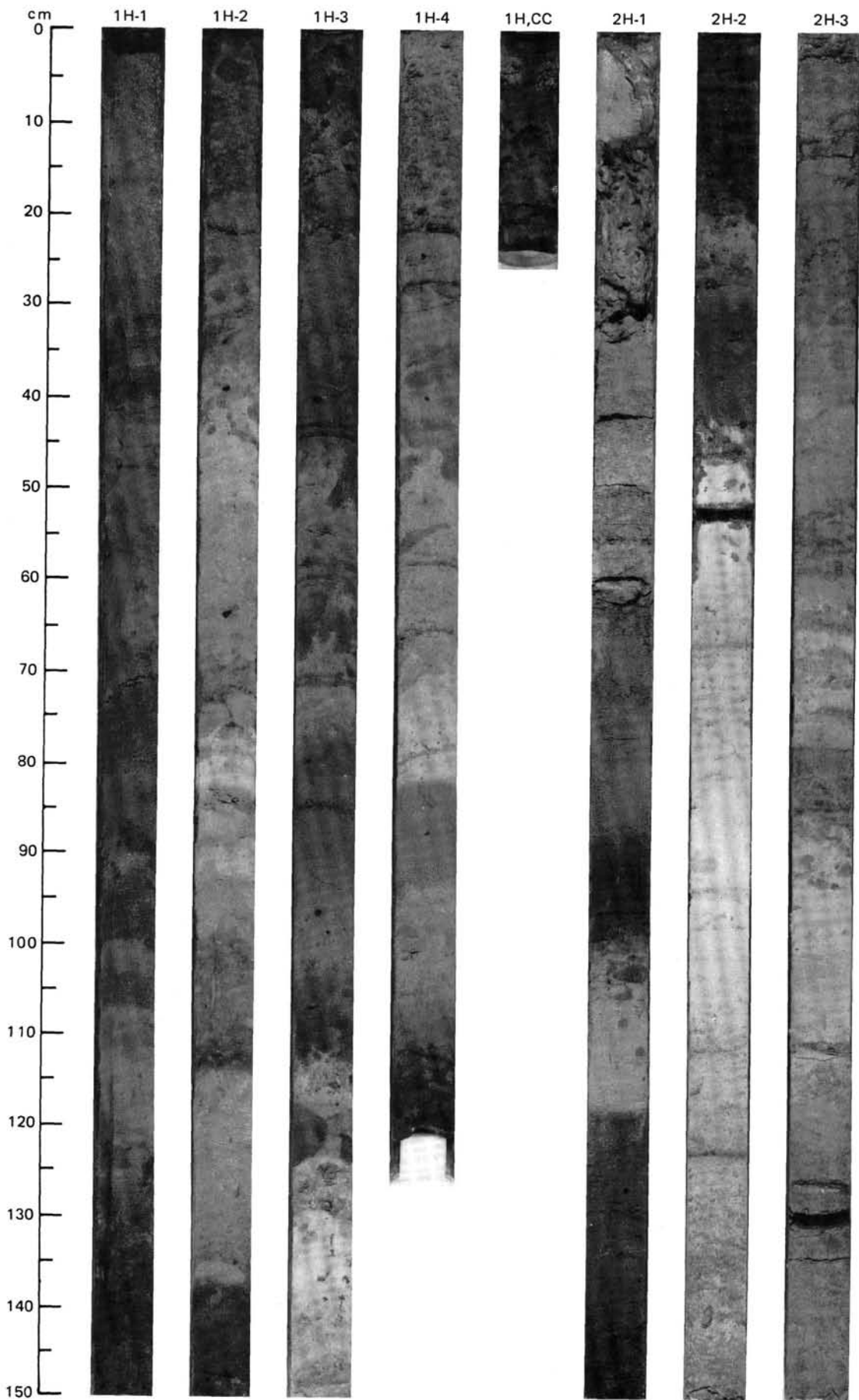
SITE 665 (HOLE A)

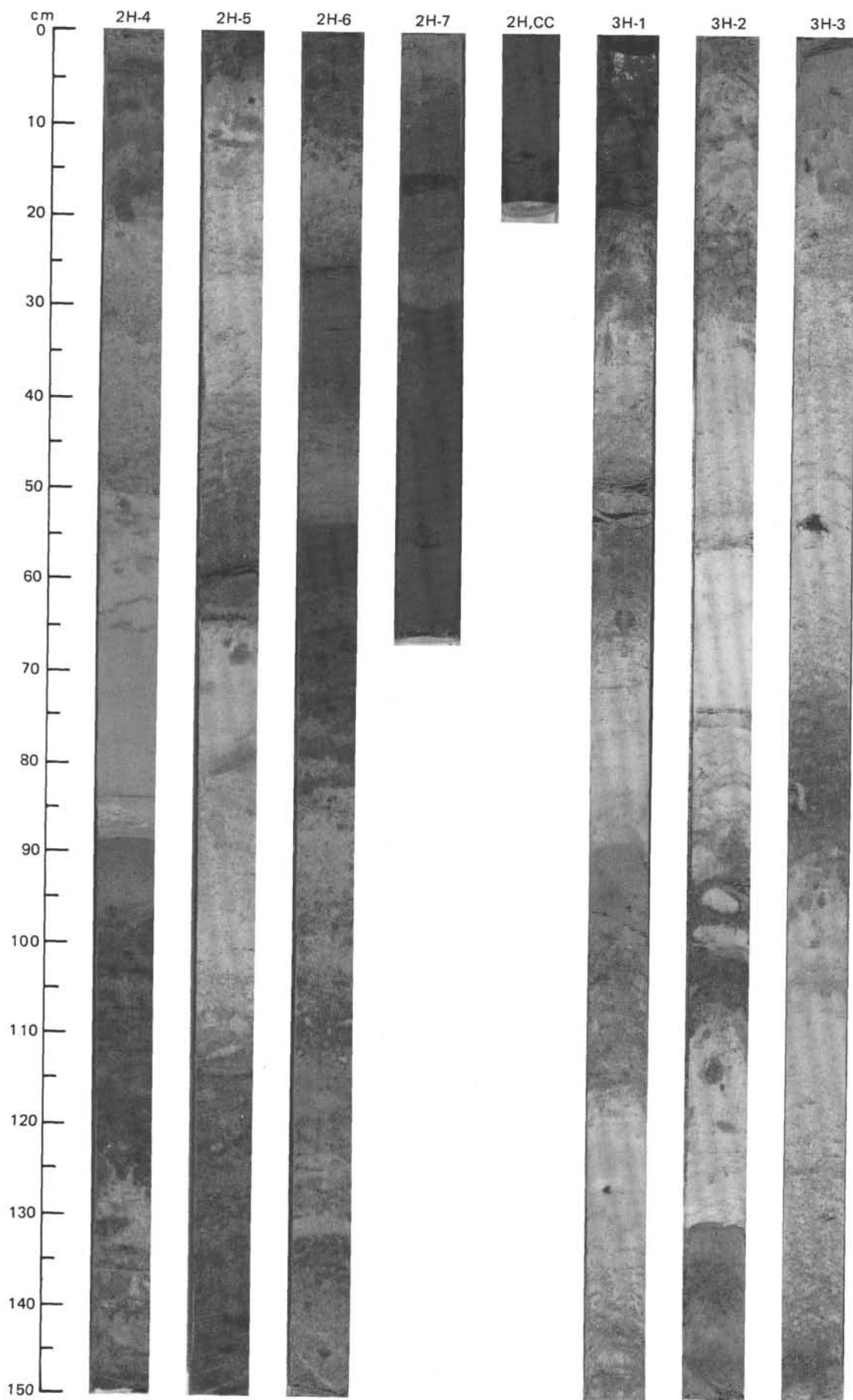


cm
0
10
20
30
40
50
60
70
80
90
100
110
120
130
140
150

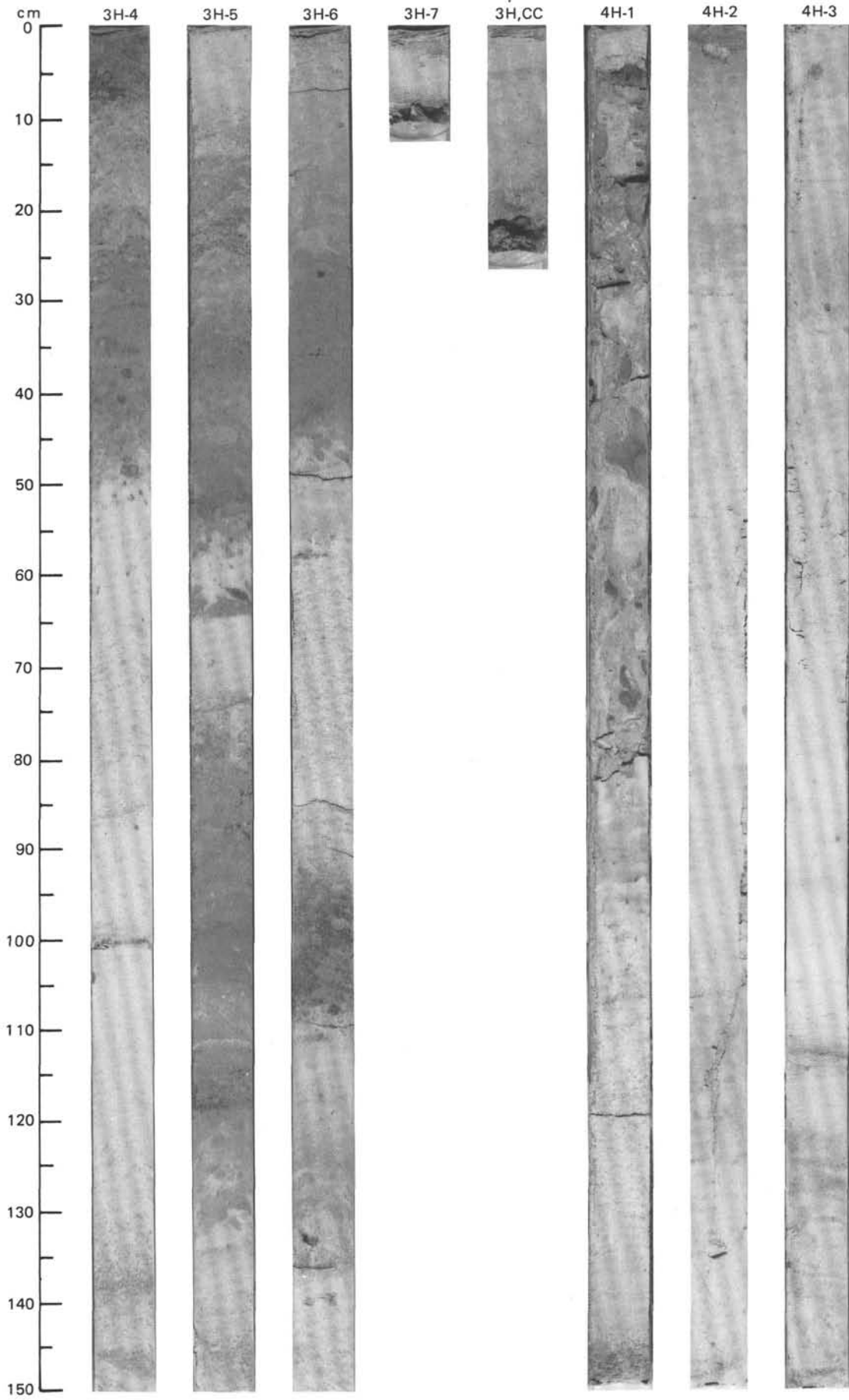


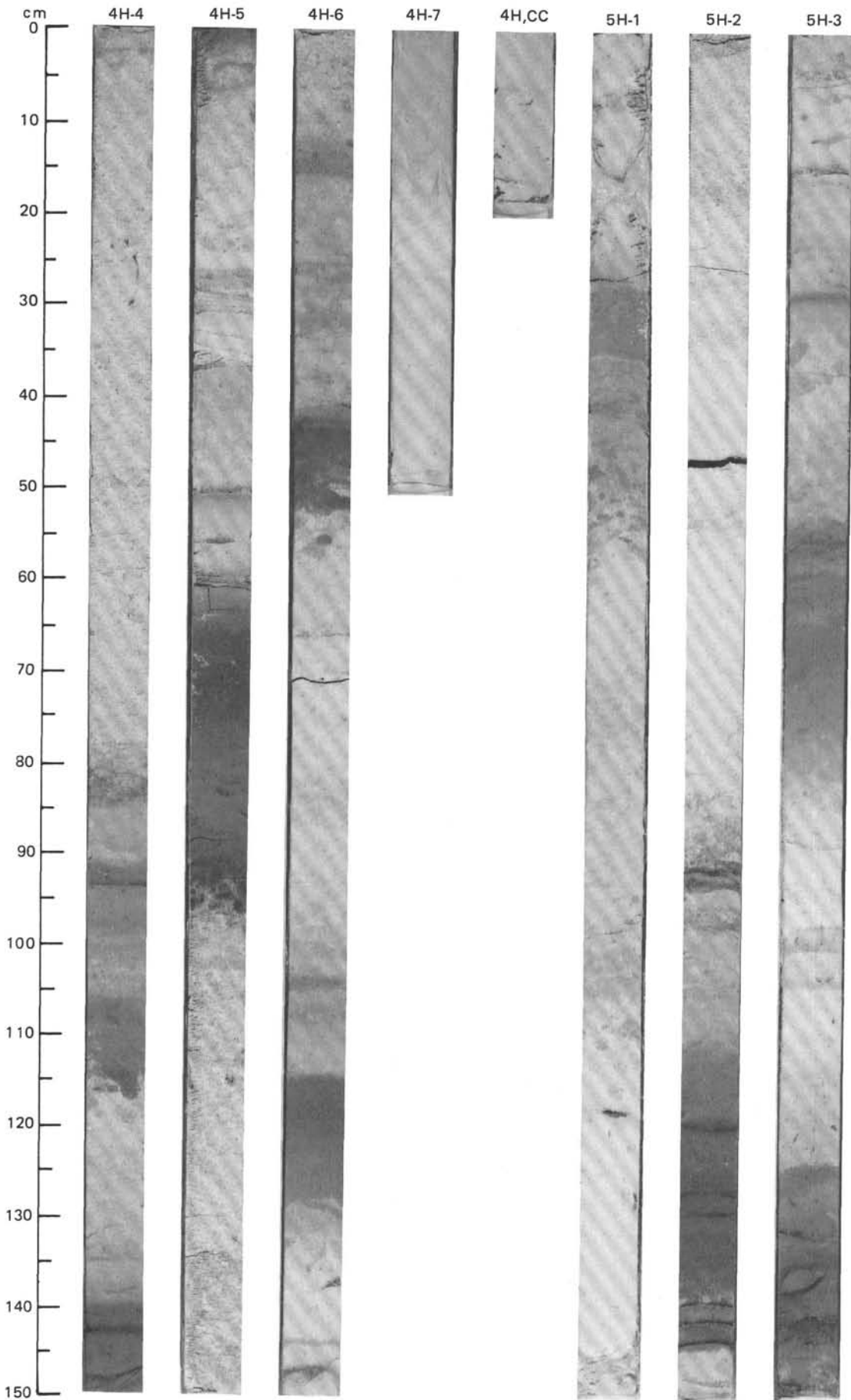
SITE 665 (HOLE B)



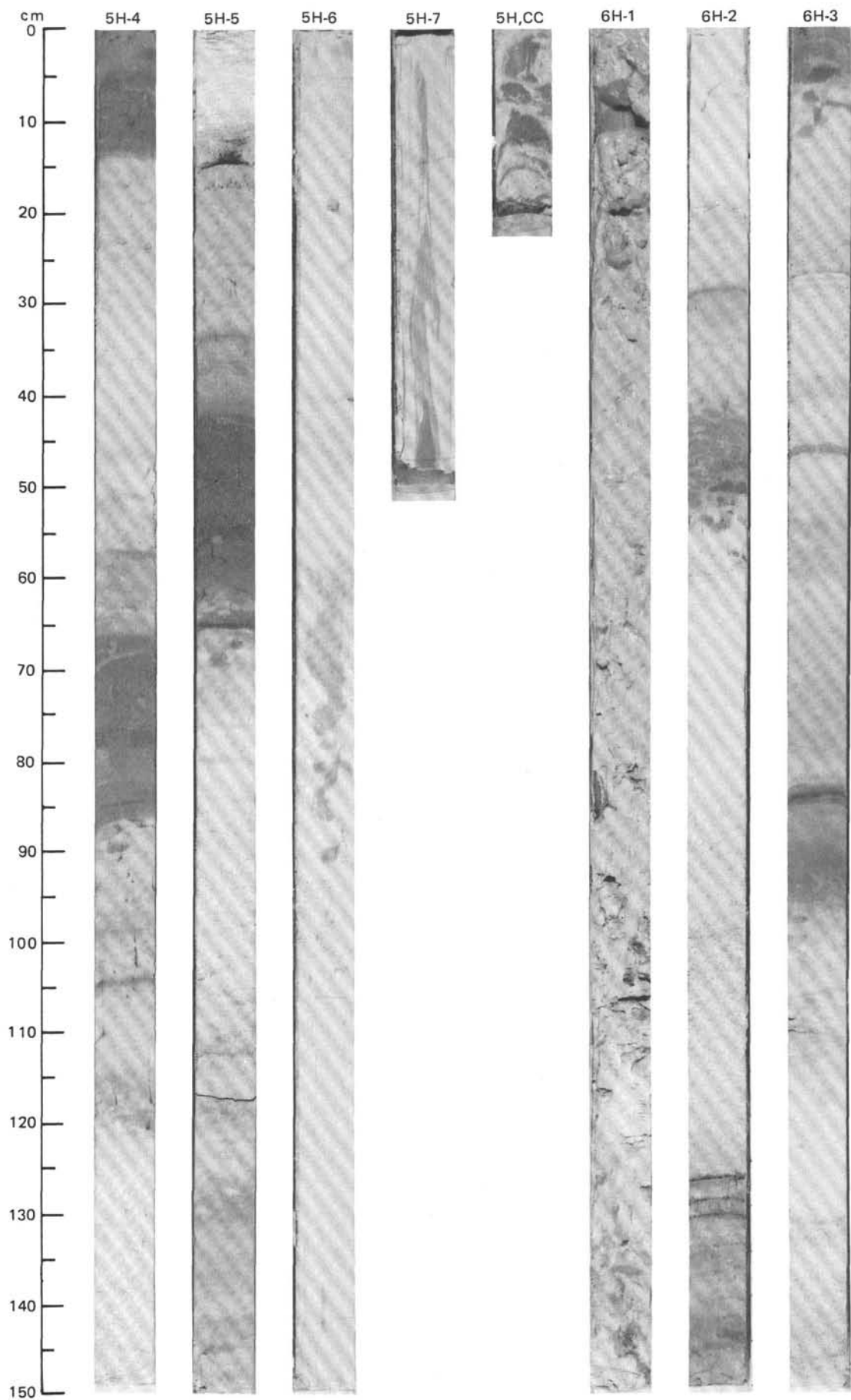


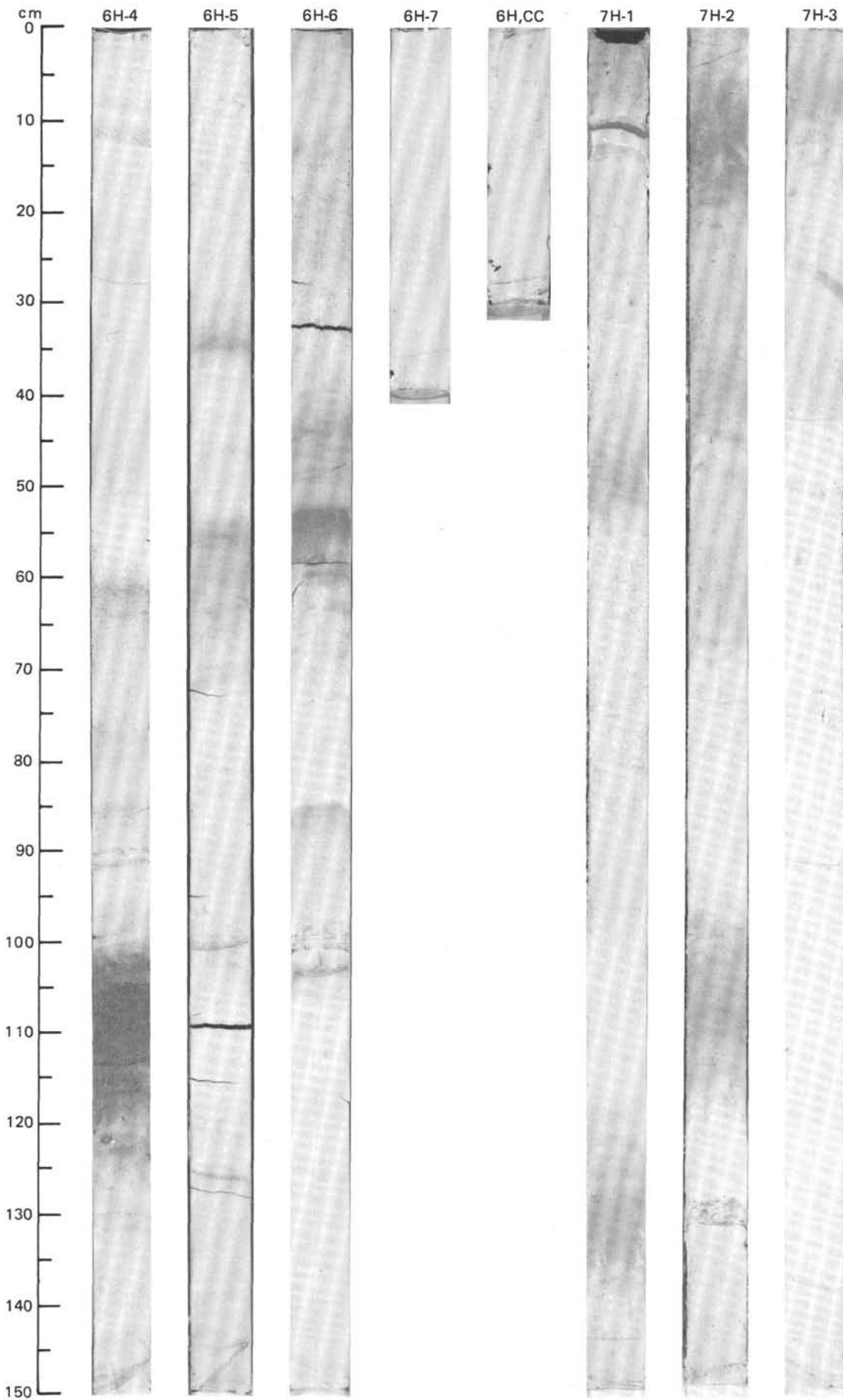
SITE 665 (HOLE B)





SITE 665 (HOLE B)





SITE 665 (HOLE B)

